scientific reports

Check for updates

OPEN

Wild grown *Portulaca oleracea* as a novel magnetite based carrier with in vitro antioxidant and cytotoxicity potential

Adina-Elena Segneanu[1,10], Gabriela Vlase[1,2], Catalin Nicolae Marin[3], Titus Vlase[1,2], Crina Sicoe[4,10], Daniel Dumitru Herea[5], Maria Viorica Ciocîlteu[6], Ludovic-Everard Bejenaru[7]✉, Anca Emanuela Minuti[5], Camelia-Mihaela Zară[5], Vlad Socoliuc[8], Cristina Stavila[5] & Cornelia Bejenaru[9]

The latest research on nanotechnology through the new tailored scaffolds encompassed the therapeutic effects of natural compounds, and the unique properties of metallic nanoparticles offer new possibilities in emerging biomedical fields. Various strategies have been developed to address the limitations of existing therapeutic agents concerning specificity, vectorization, bioavailability, drug resistance, and adverse effects. In this study, the medicinal plant *Portulaca oleracea* L. and magnetite nanoparticles were used to develop an innovative target carrier system, designed to enhance the cytotoxic effect and overcome the main drawbacks (permeability and localization) of the phytoconstituents. The low-metabolite profile of Romanian wild-grown *Portulaca oleracea* L. exhibits a diverse range of hundred fifty-five compounds across various chemical categories (amino acids, peptides, fatty acids, flavonoids, alkaloids, terpenoids, phenolic acids, organic acids, esters, sterols, coumarins, nucleosides, lignans, and miscellaneous compounds). Morpho-structural and magnetic properties of the new phytocarrier were investigated using a variety of methods, including XRD, FTIR, Raman, SEM, DLS), and magnetic determinations. The MTT assay was conducted to evaluate in vitro the potential cytotoxicity on normal human dermal fibroblasts (NHDF), as well as on two tumoral cell lines: human osteosarcoma (HOS) and cervical cancer (HeLa). Results indicated that significant inhibition of both cancer cell lines' viability was exerted by the new phytocarrier compared to herbal extract. Furthermore, the results obtained for the total phenolic content and the antioxidant potential screening performed using the FRAP and DPPH assays were superior for the new carrier system. These findings suggest the potential biomedical applications of the developed carrier system and its promising implications for future research and development in the field.

Keywords Purslane, Magnetite, Carrier system, Secondary metabolites, Antioxidant potential, In vitro cytotoxicity

[1]Department of Chemistry, Institute for Advanced Environmental Research, West University of Timişoara (ICAM–WUT), 4 Oituz Street, 300086 Timişoara, Romania. [2]Research Center for Thermal Analyzes in Environmental Problems, West University of Timişoara, 16 Johann Heinrich Pestalozzi Street, 300115 Timişoara, Romania. [3]Faculty of Physics, West University of Timişoara, 4 Vasile Pârvan Avenue, 300223 Timişoara, Romania. [4]Faculty of Chemistry, Biology, Geography, West University of Timişoara, 16 Johann Heinrich Pestalozzi Street, 300115 Timişoara, Romania. [5]National Institute of Research and Development for Technical Physics, 47 Dimitrie Mangeron Avenue, 700050 Iaşi, Romania. [6]Department of Instrumental and Analytical Chemistry, Faculty of Pharmacy, University of Medicine and Pharmacy of Craiova, 2 Petru Rareş Street, 200349 Craiova, Romania. [7]Department of Pharmacognosy & Phytotherapy, Faculty of Pharmacy, University of Medicine and Pharmacy of Craiova, 2 Petru Rareş Street, 200349 Craiova, Romania. [8]Laboratory of Magnetic Fluids, Center of Fundamental and Advanced Technical Research, The Romanian Academy–Timişoara Branch, 24 Mihai Viteazul Avenue, 300223 Timişoara, Romania. [9]Department of Pharmaceutical Botany, Faculty of Pharmacy, University of Medicine and Pharmacy of Craiova, 2 Petru Rareş Street, 200349 Craiova, Romania. [10]Adina-Elena Segneanu and Crina Sicoe contributed equally to this work. ✉email: ludovic.bejenaru@umfcv.ro

Portulaca oleracea L., purslane (*Portulacaceae* family), is the only representative of the *Portulaca* genus in Romania's spontaneous flora. It is widely distributed across all regions, from the steppe zone to hilly areas, thriving in light, sandy soils[1]. Globally, the species is found across diverse areas, and its common names vary by language and locality. For example, it is known as "rigla" in Egypt, "pigweed" in England, "pourpier" in France, and "Ma-Chi-Xian" in China[1–7]. In Romania, the plant is commonly referred to as "grașiță", "iarba-grasă", or "iarba-porcului"[1,8]. The leaves and stems are traditionally used in soups and salads in Mediterranean and Asian countries, including Romania[8,9].

Studies indicate that *P. oleracea* has been utilized in Romanian cuisine since ancient times, where it was known as "Iaca" among the Dacians[10]. Renowned for its medicinal properties, the plant has been traditionally used to treat inflammations and scurvy[1,8]. *P. oleracea* is recognized in traditional medicine across many regions for its antiseptic, anti-inflammatory, antispasmodic, anticonvulsant, diuretic, febrifuge, and vermifuge properties[11]. Its use in various cultures dates to Antiquity, as documented by Dioscorides in *Materia Medica*, Avicenna in *Canon of Medicine*, Ayurvedic and Unani medicine systems, and traditional Chinese medicine[7,12]. In Romania, "grașița" has been historically used in external baths to treat periods of weakness and illness[13].

P. oleracea contains numerous active compounds. In the aerial part of the plant, the presence of flavonoids, alkaloids, α-linolenic acid (omega-3) type fatty acids, vitamins, minerals[9,11,14], terpenoids, polysaccharides, sterols, proteins[12], catecholamines, phenolic acids, lignans, and anthocyanidins has been reported[7].

Recently, significant attention has been focused on the phytoconstituents and biological activity of *P. oleracea*[2,7,9,11–13,15]. Research has highlighted the pharmacological effects of extracts obtained from the aerial parts of *P. oleracea* plants: antimicrobial, neuroprotective, antioxidant, antidiabetic, anti-inflammatory, anticancer, antiulcerogenic, hepatoprotective activities[9,11,12,14,16,17]. However, much of the research focuses on isolating specific categories of biomolecules from different parts of the plant[4,18–20].

The medicinal plant metabolite profile is influenced by several factors, including its origin, harvest period, and the specific plant parts used[21–23]. Additionally, the extraction of phytochemicals is governed by solvent polarity, temperature, pH, and duration, among others[24,25]. Consequently, all these factors can significantly impact the correlation between phytoconstituents and their pharmacological activity, making it challenging to establish a clear relationship between them. Furthermore, numerous studies have reported that the combined therapeutic effects of all secondary metabolites and signaling molecules are significantly more effective than a single biomolecule or categories of phytoconstituents[21,22,26,27]. Thus, further research is needed to fully explore the chemical composition of this plant and its potential health benefits.

In parallel, recent advances in nanotechnology have explored the environmentally friendly synthesis of metallic nanoparticles using components of *P. oleracea*[28,29].

Magnetic nanoparticles, in particular, have become a focal point in biomedical research, especially in drug delivery, cancer diagnosis, and treatment[30–32]. The ability to control the size, shape, and surface chemistry of magnetic particles offers a strong foundation for the development of high-performance drug delivery systems. Various studies reported that surface-tailored with different moieties can enhance biocompatibility, thereby facilitating the development of performance drug delivery systems[33,34]. In addition, through surface modification with diverse biomolecules, magnetic particles can be fine-tuned to achieve highly selective targeting, thereby reducing side effects. Consequently, magnetic particle-based drug delivery systems have shown promising results, particularly in cancer therapies[35,36].

On the other hand, a well-known fact is that the morpho-structural properties of some highly bioactive phytochemicals may face challenges related to stability, adsorption, bioavailability in vivo, target specificity, and transmembrane permeability, limiting their effectiveness in treating severe diseases[22,37].

Therefore, the development of carrier systems that combine the therapeutic properties of whole plant components with the features of modern drug delivery systems is crucial to overcoming these limitations.

This study aims to explore the potential of *P. oleracea* in combination with nano-magnetite as an innovative carrier system. The research investigates its morpho-structural and magnetic properties, antioxidant potential, and the in vitro cell viability. To our knowledge, this is the first study to explore the metabolite profile of *P. oleracea* grown wild in Romania, opening new avenues for therapeutic applications.

Results

Despite the extensive research on the chemical screening and biological activity of purslane, there is insufficient research addressing the flavones, sterols, or fatty acids content of the wild-grown Romanian *P. oleracea*[38–40]. This study presents a comprehensive analysis of the herb's low metabolic profile using cutting-edge techniques, including gas-chromatography coupled with mass spectroscopy (GC–MS) and electrospray ionization–quadrupole time-of-flight–mass spectrometry (ESI–QTOF–MS). The phytoconstituents identification is based on the retention indices, the Mass Spectral Library 2.0 database, and the literature review.

GC–MS analysis of *P. oleracea* sample

The biomolecules separated via GC–MS are presented in (Fig. 1S and Table 1).

The GC–MS analysis reveals thirteen major compounds, constituting approximately 84% of the total peak area in the *P. oleracea* sample (Fig. 1S).

Mass spectrometry analysis of *P. oleracea* sample

The mass spectra depicted in Fig. 2S provide clear evidence of a wide array of phytochemicals. Some of these compounds have been detected and assigned various chemical classes, including amino acids, peptides, fatty acids, flavonoids, alkaloids, terpenoids, phenolic acids, organic acids, esters, sterols, coumarins, nucleosides, lignans, and miscellaneous constituents. These findings are consistent with the literature[41–64].

The phytoconstituents identified via ESI–QTOF–MS analysis are presented in (Fig. 2S and Table 1S).

No	Retention time (t_R)	Retention index (RI)	Area (%)	Compound name	Ref
1	3.11	822	4.15	2-hexenal	[41]
2	4.39	946	0.16	Benzaldehyde	[42]
3	5.73	3643	6.26	Ursolic acid	[43]
4	9.65	1225	9.37	Cuminaldehyde	[44]
5	10.54	1021	4.08	Limonene	[44–47]
6	11.63	1488	5.23	β-ionone	[45]
7	16.18	1090	0.42	Linalool	[43,45]
8	19.25	1546	8.98	β-caryophyllene	[43,45]
9	20.54	1609	20.29	Methyl tridecanoate	[43,45]
10	21.23	1241	8.45	Carvone	[43,45]
11	22.87	3219	1.49	Lupeol	[47]
12	36.65	3295	17.29	Campesterol	[47]
13	37.17	3289	1.98	β-sitosterol	[47]

Table 1. Main phytochemicals identified by GC–MS analysis of the *P. oleracea* sample. *RI* retention indices calculated based upon a calibration curve of a C8–C20 alkane standard mixture.

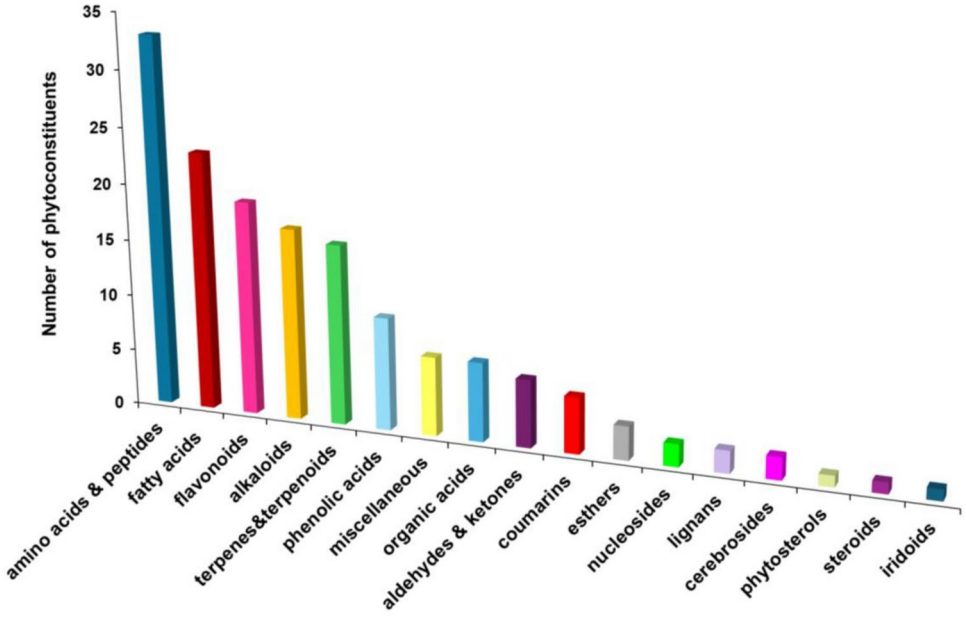

Fig. 1. Phytoconstituents classification bar chart of *P. oleracea* sample.

Screening and classification of the differential phytochemicals

A total of 155 phytoconstituents identified through mass spectroscopy were assigned to different chemical classes: amino acids and peptides (21.29%), fatty acids (14.83%), flavonoids (12.25%), alkaloids (10.96%), terpenes and terpenoids (10.32%), phenolic acids (6.45%), organic acids and esters (6.45%), coumarins (3.22%), sterols (1.29%), nucleosides (1.29%), lignans (1.29%), and miscellaneous. Figure 1 presents the classification chart of the biomolecules from the *P. oleracea* sample based on the data analysis reported in (Table 1S).

According to Fig. 1, amino acids and peptides constitute the largest category of phytochemicals, accounting for approximately 21.29% of them. This category comprises six essential amino acids, namely isoleucine, lysine, methionine, phenylalanine, threonine, and tryptophan, as well as non-essential amino acids such as alanine, glycine, arginine, histidine, serine, tyrosine, cystine, proline, glutamic acid, and aspartic acid. It is noteworthy that around 53% of these biomolecules, including phenylalanine, arginine, isoleucine, tryptophan, alanine, glutamic acid, histidine, cysteine, and glycine, are involved in mechanisms of antiproliferative, cytotoxic, and immunomodulating activities[65–74]. Moreover, other compounds from this category (methionine, proline, serine, lysine, and threonine) exhibit anti-inflammatory activity, accounting for approximately 30% of the total[75–80]. The analysis of a *P. oleracea* sample revealed the presence of 16 small peptides consisting of di- and tripeptides. Recent research has reported on the pharmacological potential of small peptides from plants, which have demonstrated antitumoral, antiviral (anti-HIV), antimicrobial, antifungal, antioxidant, antidiabetic, and neuro-regulatory properties[81].

Fatty acids constitute the second largest group, comprising a staggering 14.83%. This group encompass thirteen saturated fatty acids (caproic, lauric, myristic, pentadecanoic, palmitic, margaric, stearic, arachidic, henicosanoic, behenic, tricosanoic, lignoceric and cerotic acid), ten unsaturated acids or essential oils namely six omega-3 acids (alpha-linoleic, eicosapentaenoic, eicosatrienoic, docosahexaenoic, stearidonic and docosapentaenoic acid) and two omega-6 acids (linolenic and arachidonic acid), and two monounsaturated fatty acids (oleic and palmitoleic acid). Fatty acids have been the subject of extensive research, and their numerous health benefits include cardioprotective, neuroprotective, antibacterial, antifungal, anti-inflammatory, antioxidant, immunomodulatory, and neuroprotective effects[82,83].

Flavonoids are another important category of metabolites with a significant array of therapeutic attributes, such as antioxidant, anti-inflammatory, cardioprotective, neuroprotective, antimicrobial, antiviral, and antitumoral activities[84,85].

Alkaloids constitute a significant proportion, precisely 10.96%, of the total phytochemical content from the *P. oleracea* sample. These metabolites exhibit remarkable therapeutic potentials, such as antitumoral, neuroprotective, antidiabetic, hypoglycemic, antioxidant, anticholinesterase, and other properties[53,86,87].

Terpenes and terpenoids are a class of secondary metabolites exhibiting broad biological properties. They possess potent antimicrobial, antiviral, anti-inflammatory, antitumor, neuroprotective, cardioprotective, analgesic, antispasmodic, antihyperglycemic, immunomodulatory, and other effects[88].

Phenolic acids account for 6.45% of the herb's phytoconstituents. Various studies have revealed their potential as antioxidant, antimicrobial, cardioprotective, anti-inflammatory, neuroprotective, antitumor, and antidiabetic agents[89].

Coumarins are metabolites highly relevant to human health. Recent studies have conclusively shown that coumarins possess highly antioxidant, antimicrobial, anticancer, anti-inflammatory, anti-angiogenic, anti-oxidative, antidiabetic, antihypertensive, hepatoprotective, neuroprotective, and immunomodulatory effects[87,89,90].

Phytosterols are secondary compounds that act as neuroprotective, immunomodulatory, antioxidant, anti-inflammatory, cardiovascular protective (lowering LDL-cholesterol concentrations), immunomodulatory, and antitumoral agents[91].

Lignans are a class of phytochemicals that exhibit a range of pharmacological properties. These compounds possess antioxidant, antibacterial, antiviral, fungicidal, insecticidal, estrogenic, and antitumor activities[92].

The VOC flavor profile of phytoconstituents identified in the *P. oleracea* sample is depicted in (Table 2S and Fig. 3S).

Phytocarrier system

Despite their significant biological activity, different secondary metabolites display lower bioavailability and stability in vivo[4,45] Therefore, the tailored engineered scaffold development to address these challenges successfully opens new opportunities in the biomedical field. Accordingly, a new phytocarrier system was prepared based on the loading of magnetite nanoparticles into *P. oleracea* phytochemicals, aiming to exploit the synergistic effects of both constituents and thereby enhance their pharmacological potential.

Fourier transform infrared (FTIR) spectroscopy

The surface area modification of magnetite particles using herb components and the PM carrier system preparation was investigated through FTIR spectroscopy. The obtained spectra for both the herb sample and the phytocarrier system are displayed in (Fig. 2).

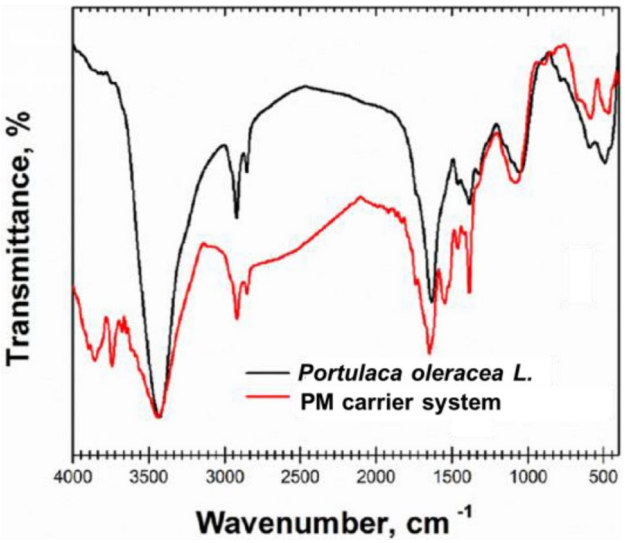

Fig. 2. FTIR spectra of *P. oleracea* and new phyto-nanocarrier system.

Phytoconstituent category	Wavenumber (cm^{-1})	Ref
Amino acids	3400, 3328–3130, 2983, 2360, 2130, 1726–1753, 1692, 1676, 1667, 1651, 1644, 1632, 1628, 1612, 1501–1602	93
Fatty acids	3604, 3022–3008, 2962, 2927, 2874, 2848, 1700, 1349, 1243, 725	45
Alkaloids	3358, 1589, 1644, 1405, 1377, 740, 662	45
Terpenoids	2945, 1748, 1708, 1651, 812	94
Flavonoids	3880–3126, 3142–2978, 1657, 1645, 1618, 1583, 1495, 1464, 1418, 1369, 1273, 1082, 771, 533	45
Phenolic acids	1788, 1728, 1665, 1641, 1519, 1442, 1409, 1363, 1310, 1263, 1164, 1089, 947, 806	94,95
Iridoids	1740–1458, 1377, 1221–914	89
Phytosterols	3427, 3348, 2935, 2830, 1755, 1640, 1461, 1384, 1188, 1063, 990, 945, 882, 741	94,96
Lignans	2990, 2924, 2876, 2831, 1615, 1498, 1430, 1385, 1355, 1327, 1274, 1266, 1101, 1047, 1007, 992, 930	97
Nucleosides	3352, 3103, 2927, 2802, 1669, 1472, 1393, 1272, 1208, 1142, 1097, 1056, 977, 904, 830, 773, 567, 451	94,98
Iridoids	3355, 2915, 1650, 1487, 1362, 1055, 1010	99

Table 2. Characteristic vibrational frequencies attributed to the phytoconstituents from the *P. oleracea* sample.

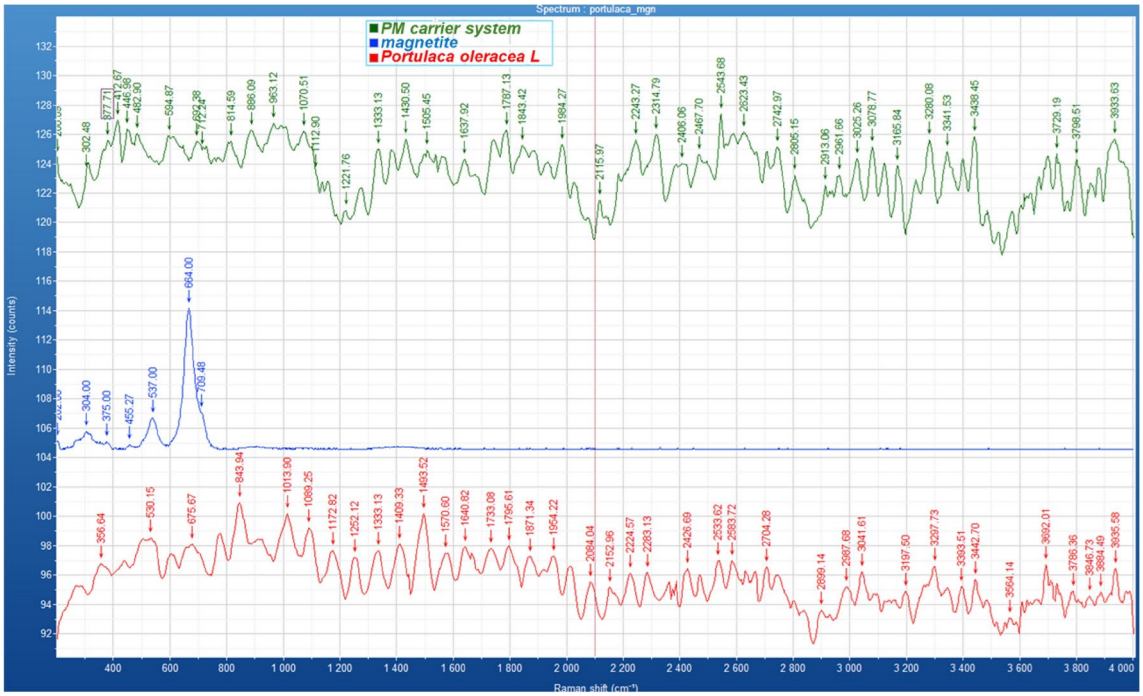

Fig. 3. Raman spectrum of *P. oleracea*, magnetite, and PM carrier system.

The analysis of the *P. oleracea* pattern sample (Table 2) revealed the presence of characteristic vibrational bands attributed to different phytoconstituent categories, including amino acids and peptides, alkaloids, fatty acids, flavonoids, phenolic acids, and phytosterols in the herb sample.

The absorption bands present in the spectra are characteristic of the phytoconstituents from the *P. oleracea*, including peaks at 2918 cm^{-1} (C–H stretching), 1728 cm^{-1} (C = O stretching), 1244 and 1014 (C–N of amine), 881 and 819 cm^{-1} (C–O and CH vibration of aromatic rings). The Fe–O stretching vibrations, attributed to magnetite, are also evident at 632, 585, and 474 cm^{-1}[100–103]. However, changes in the intensity of OH, C–O, and N–H regions (1567, 1386, 1248, 1204 cm^{-1}) are observed. These changes are accompanied by a shift towards higher wavenumbers in the (O–H, N–H, and C–O) corresponding regions, indicating that these functional groups are involved in the phyto-nanocarrier formation. Additionally, the Fe–O bond vibration of Fe_3O_4 nanoparticles confirms the integration of the herb biomolecules into the pores of magnetite nanoparticles.

Raman spectroscopy

The Raman spectral analysis (Figs. 3 and 4S) provides compelling evidence of the successful interaction between magnetite nanoparticles and *P. oleracea* biomolecules, confirming the formation of a novel phytocarrier system with enhanced structural and functional properties.

In the Raman spectra of magnetite nanoparticles (Fig. 3), the characteristic vibrational bands of Fe_3O_4 are observed at approximately 202, 304, 375, 455, and 664 cm^{-1}, aligning well with reference data and validating both the purity and structural integrity of the material[104].

In the PM carrier system, the Raman spectra (Figs. 3 and 4S–b) retain key magnetite-associated peaks at 202, 304, and 377 cm^{-1}, confirming the preservation of the magnetic phase within the newly developed carrier. A particularly noteworthy observation is the distinct shift of the magnetite vibrational bands (455, 537, 664, and 709 cm^{-1}) toward higher frequencies in the PM carrier system compared to the pure magnetite nanoparticles. This spectral shift strongly suggests the formation of interfacial interactions, likely mediated by chemical bonding or surface modifications resulting from the incorporation of *P. oleracea* biomolecules. Such interactions, potentially driven by coordination bonds, electrostatic forces, or hydrogen bonding, contribute significantly to the enhanced stability, dispersibility, and overall functional performance of the carrier system[105–107].

Further substantiating this integration, a comparative analysis between the PM carrier system (Figs. 3 and 4S–b) and the herb alone (Figs. 3 and 4S–a) reveals substantial peak shifts in the Raman spectra. The characteristic vibrational peaks of the herb at 844 cm^{-1} (C–H bending), 1495 cm^{-1} (C–O stretching), 1795 cm^{-1} (C = O amidic), and 3280 cm^{--1} (O–H stretching) undergo pronounced frequency shifts to 886, 1505, 1843, and 3341 cm^{-1}, respectively, in the PM carrier system. These significant spectral variations indicate the new intermolecular interaction formation between the phytochemical constituents of *P. oleracea* and the magnetite nanoparticles, further reinforcing the structural integrity of the composite[108,109]. The observed spectral modifications confirm the successful integration of the two components and highlight the pivotal role of phytochemicals in stabilizing and modifying the surface properties of the magnetite nanoparticles. This structural adaptation, combined with the synergistic integration of magnetic functionality and the herb's bioactive compounds, is expected to significantly enhance the performance of the PM carrier system. The resulting composite is expected to exhibit improved stability, bioavailability, and a wide range of potential applications, making it a promising candidate for future research and development.

X-ray diffraction spectroscopy

The X-ray diffraction (XRD) patterns of *P. oleracea*, magnetite, and the new phytocarrier are shown in (Fig. 4). The diffraction pattern of the *P. oleracea* sample (Fig. 4), in the range of 13.8–41°, displays a wide band and feeble diffraction peaks attributed to amorphous phases associated with herb minerals and fibers. XRD patterns of the magnetite sample (Fig. 4) indicated the presence of distinctive peaks at (111), (220), (311), (222), (400), (422), (511), and (440) planes assigned to monocrystalline iron oxide nanoparticles with an average crystallite size of 14.9 nm[101–103].

The XRD analysis of the PM nanocarrier reveals the appearance of distinctive diffraction peaks that correspond to the characteristic peaks associated with *P. oleracea* and magnetite. The crystallite average size of 40.1 nm calculated using the Scherrer equation provides strong evidence of the successful preparation of the new phytocarrier.

Scanning electron microscopy (SEM)

The SEM micrographs of the herb, magnetic nanoparticles, and the PM carrier system are shown in (Fig. 5a,b).

The SEM analysis of the *P. oleracea* (Fig. 5a) reveals a porous structure consisting of particles of varying shapes and sizes, with an average size of approximately 100 nm. This unique nanoscale porosity creates an ideal matrix for integrating magnetite nanoparticles while maintaining the herb's natural architecture. This design enhances interactions with bioactive compounds, positioning it as a highly promising functional carrier system.

The newly developed phytocarrier system (Fig. 5b), incorporating spherical magnetic nanoparticles averaging 15 nm, shows their successful integration both on the surface and within the herb's porous structure. This ensures effective nanoparticle loading and enhances the stability and performance of the system, as the interfacial interactions are key to its functionality.

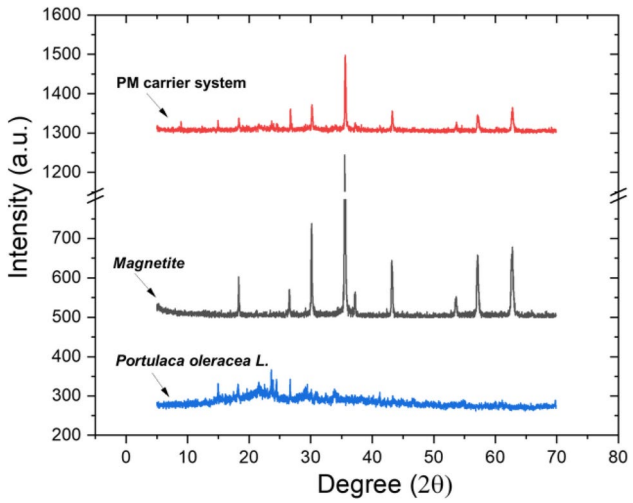

Fig. 4. Powder XRD patterns of *P. oleracea*, magnetite, and PM phytocarrier system.

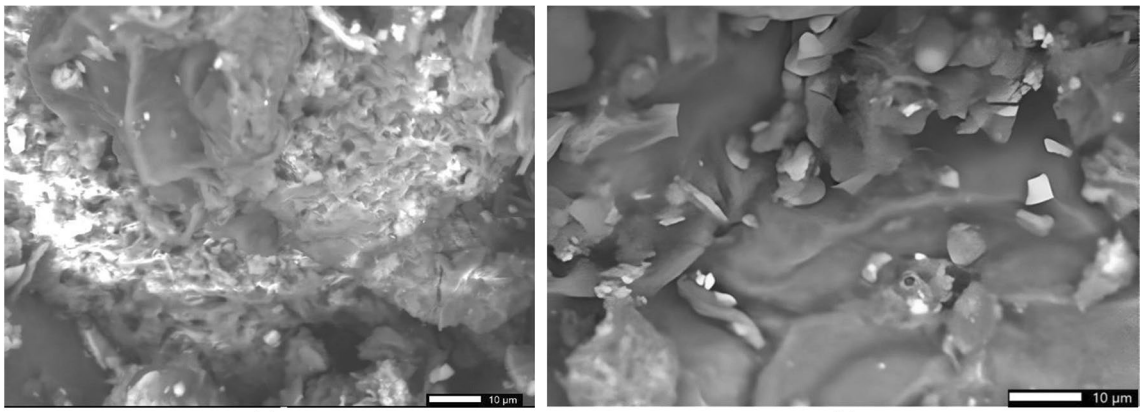

Fig. 5. SEM images of the *P. oleracea* (**a**), and the PM phytocarrier (**b**).

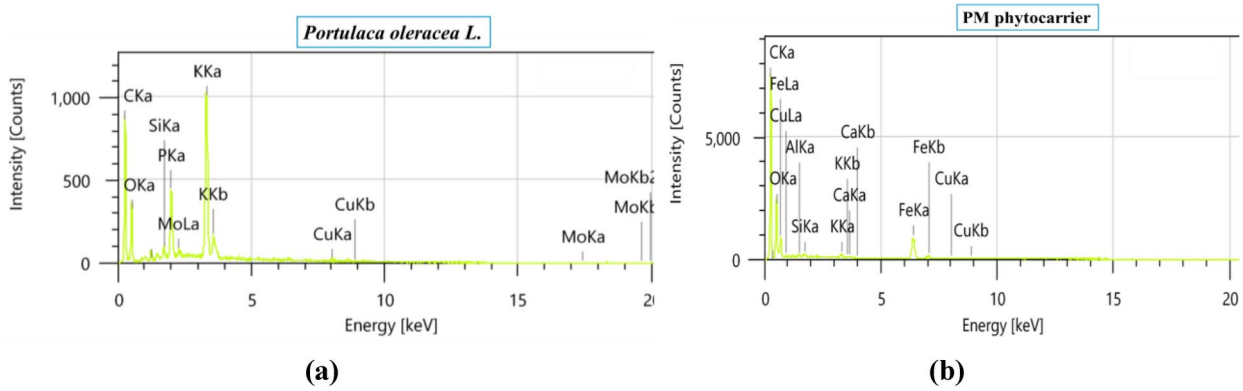

Fig. 6. EDX composition of *P. oleracea* (**a**) and PM phytocarrier (**b**).

Recent studies highlight the increasing interest in microscale carriers for biomedical applications due to their advantages in controlled drug delivery, tissue engineering, and diagnostic systems. Microscale carriers not only enable localized delivery, reducing off-target effects, but they also enhance patient outcomes in chronic disease management and regenerative medicine[110–112].

Furthermore, the incorporation of magnetic or stimuli-responsive elements allows for externally controlled drug release and targeted therapy, further enhancing their application in fields like cancer treatment. Moreover, their ability to mimic the extracellular matrix promotes cell adhesion and tissue regeneration, making them invaluable for regenerative medicine. In diagnostic imaging, functionalization with contrast agents significantly improves detection sensitivity[113,114].

Energy dispersive X-ray (EDX)

The elemental and compositional of the *P. oleracea* and the new phytocarrier were investigated using EDX technique (Fig. 6a,b).

The EDX spectra of the novel carrier system exhibit discernible peaks corresponding to *P. oleracea* (Fig. 6a) and magnetite (Fig. 6b), thereby substantiating the successful development of the new carrier system.

Dynamic light scattering (DLS)

The investigation of the stability and dynamics of a recently developed phytocarrier employed the DLS technique to ascertain the average mean particle size, as detailed in (Table 3S), and the distribution profile of all samples, as illustrated in (Fig. 7a–c).

The DLS analysis of the *P. oleracea* sample (Fig. 7a) offers valuable insights into its colloidal stability and structural composition. The results reveal three distinct peaks corresponding to porous formations, a reticular-like network, and discrete herb particles, each exhibiting different hydrodynamic diameters, as detailed in (Table 3S). The polydispersity index (PDI) values for these structures are 0.134, 0.113, and 0.0859, respectively. The first two structures demonstrate moderate PDI values, indicating a well-dispersed system with controlled heterogeneity, while the lower PDI of the herb particles suggests a more uniform and narrowly distributed population, enhancing stability and minimizing the risk of uncontrolled agglomeration. Furthermore, the DLS analysis reveals that the magnetite sample has an average mean diameter of approximately 22.5 nm[115],

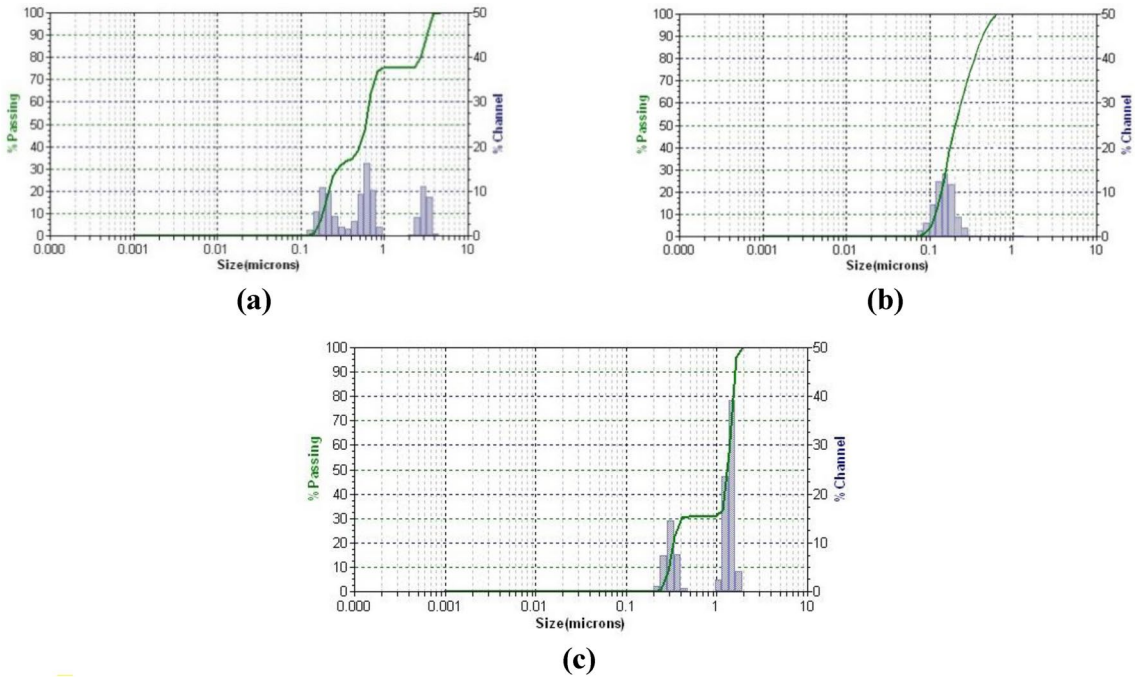

Fig. 7. DLS patterns of *P. oleracea* (**a**), magnetite (**b**), and PM phytocarrier system (**c**) in water.

with a PDI of 0.211. This moderately dispersed distribution reflects a balance between particle uniformity and some degree of size variation. The presence of magnetite nanoparticles within the dispersion is particularly noteworthy, as their interactions may influence overall stability. These particles can either enhance or hinder aggregation depending on external conditions such as pH, ionic strength, and temperature, further impacting the stability and performance of the system. Additionally, Fig. 7c illustrates the PM carrier system, which exhibits two well-dispersed peaks within a narrow range, with remarkably low PDI values of 0.0566 and 0.0928. These values indicate a highly stable system with minimal aggregation, ensuring the functional integrity of the carrier system. Notably, a shift in the mean diameter of both the magnetite and herb components suggests the successful incorporation of magnetic nanoparticles into the herb's porous and reticular-like structures. This structural adaptation likely enhances dispersion stability by preventing particle settling and maintaining a uniform suspension.

These findings align with the results of the SEM study, which further confirms the successful integration of magnetite nanoparticles within the herb matrix. The combined DLS and SEM analyses provide strong evidence of a well-structured, stable, and highly dispersed PM carrier system, highlighting its potential for various functional applications.

Magnetic properties

Figure 8a,b provides a comprehensive magnetic characterization of the PM carrier system and magnetite nanoparticles, offering key insights into their magnetic behavior, stability, and potential applications.

The hysteresis loop analysis (Fig. 8a, inset) reveals key magnetic parameters of the PM carrier system, which exhibits a saturation magnetization (Ms) of 20.9 emu/g, a coercive field (Hc) of 7 kA/m, and a remanent magnetization (Mr) of 2.6 emu/g. In contrast, magnetite shows a significantly higher Ms of 66.7 emu/g, the same Hc of 7 kA/m, and a slightly increased Mr of 7.7 emu/g. The substantial difference in Ms values indicates that the herbaceous matrix within the PM carrier system effectively dilutes the overall magnetic response, likely due to the presence of non-magnetic organic components.

Interestingly, both materials exhibit low remanent magnetization ratios (Mr/Ms) of 0.12 for the PM carrier system and 0.11 for magnetite, suggesting that their magnetization can be easily reoriented upon the removal of an external magnetic field. This behavior is highly favorable for applications requiring rapid magnetic response with minimal residual magnetization, such as targeted drug delivery, magnetic separation, and biomedical applications[116].

The Fe_3O_4 particle size plays a crucial role in determining its magnetic domain structure and overall behavior. The critical size for superparamagnetic behavior in Fe_3O_4 is typically below 20 nm, while the transition to a multi-domain state theoretically occurs between 76 and 128 nm, depending on particle shape[117].

With an average particle size of ~ 40 nm (as determined by XRD data), both the PM carrier system and magnetite nanoparticles exhibit a hysteretic profile characteristic of the single-domain regime. This regime is defined by uniform magnetization direction and high coercivity, ensuring stable magnetic properties without transitioning into a superparamagnetic state. This property is particularly advantageous for biomedical applications, such as hyperthermia therapy, where stable magnetization and heat generation under an alternating magnetic field are crucial[116].

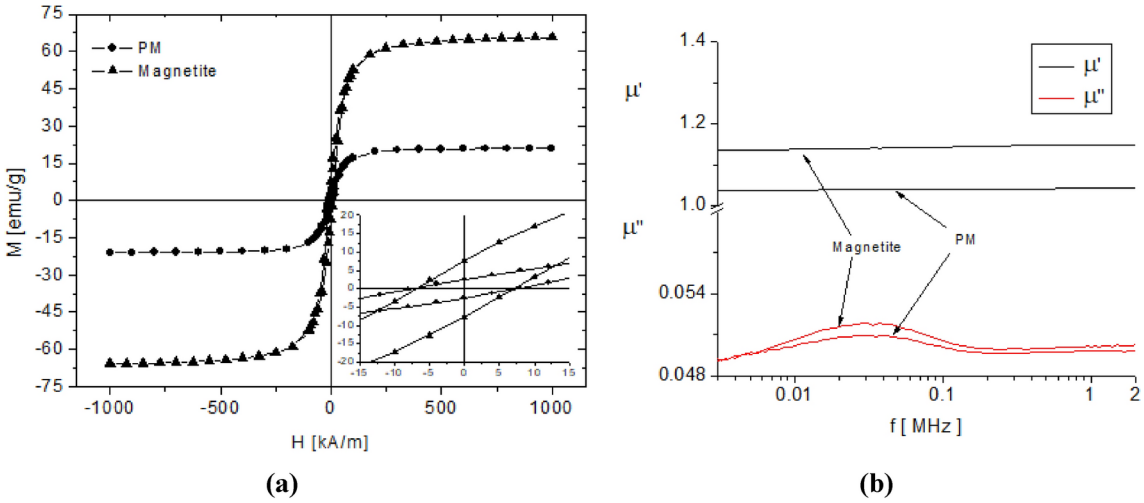

Fig. 8. Hysteresis loop of the PM carrier system and magnetite (**a**); frequency dependence of the complex magnetic permeability of the PM carrier system and magnetite (**b**).

Further insights are gained through frequency-dependent complex magnetic permeability analysis (Fig. 8b), which reveals a relaxation peak of μ′′(f) around 30 kHz for both the PM carrier system and magnetite. This peak corresponds to Néel relaxation, a process where the internal magnetic moments of nanoparticles rotate to overcome the magneto-crystalline anisotropy energy barrier. The presence of Néel relaxation in the radiofrequency range (30 kHz) indicates that these nanoparticles retain their single-domain structure while enabling efficient magnetic energy dissipation. Additionally, the absence of a multi-domain structure is confirmed by the small particle size, which restricts domain wall formation, further ensuring stable and predictable magnetic behavior. The presence of Néel relaxation in the radiofrequency range highlights the potential of the PM carrier system for applications such as magnetic hyperthermia, smart nanocarriers, etc.[116].

Overall, the combined hysteresis and permeability analyses confirm that despite its reduced overall magnetization due to the herbaceous matrix, the PM carrier system maintains essential magnetic functionalities, balancing sufficient magnetization for external manipulation with high responsiveness and stability[103]. While magnetite nanoparticles offer superior magnetic performance, the PM carrier system provides a biocompatible alternative with controlled magnetic properties, making it a promising candidate for biomedical and environmental applications where moderate yet stable magnetic behavior is required.

Screening of antioxidant activity

To assess the antioxidant potential of a medicinal plant, selecting a minimum of three appropriate assays is required[118].

In vitro tests are often the preferred method due to their simplicity, speed, and reliability, making them ideal for estimating the antioxidant activity of complex matrices[118].

The PM carrier system antioxidant potential arises from the combined influence of all biomolecules from the plant and the magnetic component. Therefore, three tests (total phenolic content (TPC)—Folin–Ciocalteu assay, ferric reducing antioxidant power (FRAP), and DPPH) were employed to assess the new carrier system antioxidant potential. The results are presented in (Fig. 9a–c).

The TPC, as determined by the Folin-Ciocalteu assay (Fig. 9a), revealed that the PM carrier system exhibited a significantly higher total phenolic content (12.16 ± 0.26 mg/g GAE) compared to *P. oleracea* (10.70 ± 0.11 mg/g GAE), representing a 20.18% increase ($p < 0.001$). This statistically significant enhancement suggests that the magnetic component of the PM carrier system acts as a catalytic agent, facilitating the release and stabilization of polyphenolic compounds, thereby improving their bioavailability[119]. Given the essential role of polyphenols in antioxidant activity, these findings support the hypothesis that the PM carrier system optimizes both the stability and functionality of bioactive compounds, ultimately enhancing antioxidant potential. Statistical validation through a one-way analysis of variance (ANOVA) followed by Dunnett's multiple comparison post hoc test confirmed the robustness of this enhancement ($p < 0.001$). Furthermore, the effect size (Cohen's $d > 0.8$) suggests a large and biologically relevant effect, reinforcing the efficacy of the PM carrier system in enhancing polyphenolic content.

Similarly, the FRAP assay (Fig. 9b) demonstrated that the PM carrier system exhibited significantly greater reducing power (31.61 ± 0.001 mM Fe^{2+} equivalent) compared to *P. oleracea* (25.23 ± 0.14 mM Fe^{2+} equivalent), with statistical significance ($p < 0.05$). This 25.28% increase in reducing power indicates a stronger ability to reduce Fe^{3+} to Fe^{2+}, a key mechanism in antioxidant defense. The effect size calculated using Cohen's $d = 1.05$ (large effect size) and partial eta squared ($\eta^2 = 0.59$, strong effect), further underscores the substantial impact of the PM carrier system on redox potential. This increase is likely attributed to the improved stabilization and bioavailability of redox-active polyphenolic compounds facilitated by the presence of magnetite nanoparticles[120].

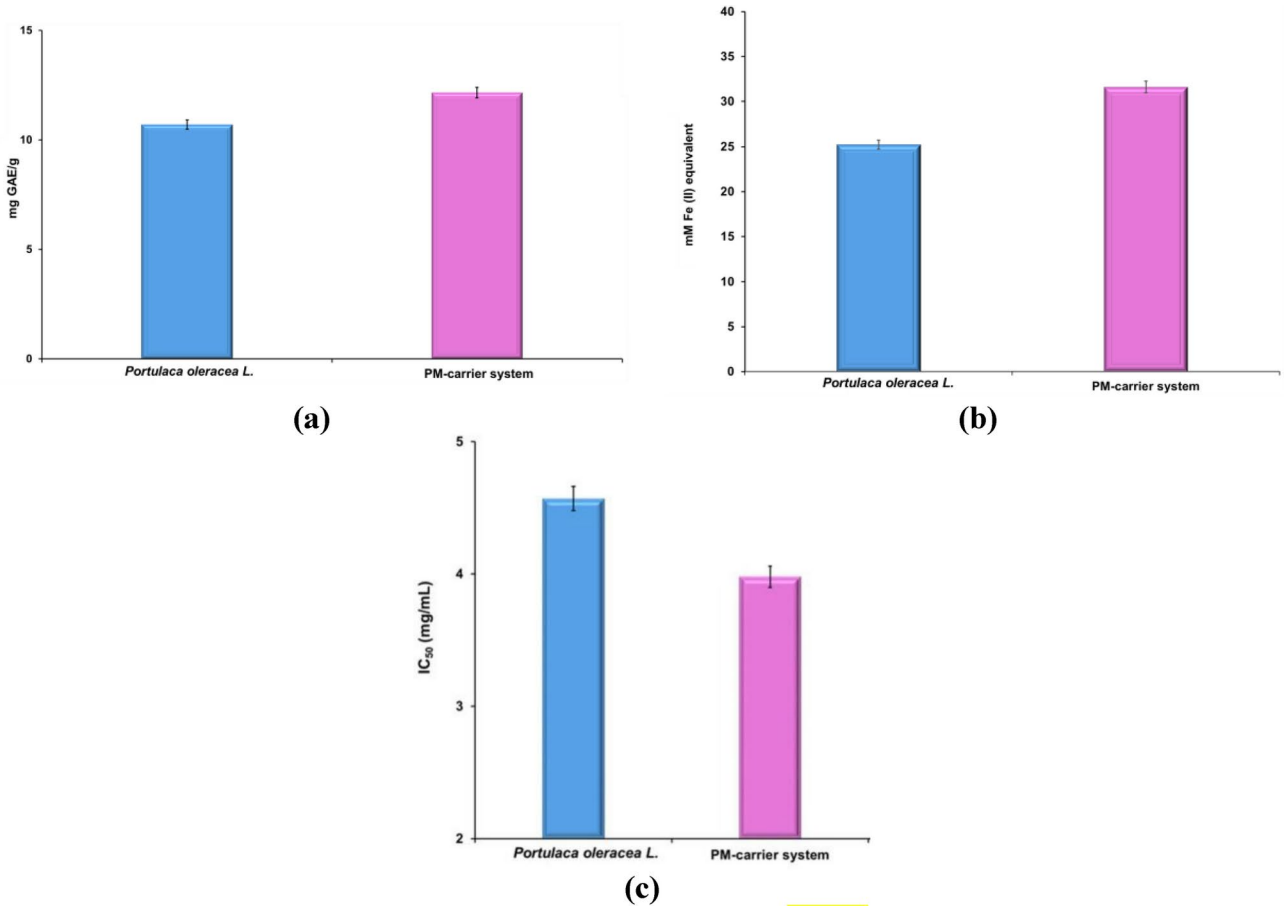

Fig. 9. Graphic representation of total phenolic content (TPC) (**a**), FRAP (**b**), and DPPH (**c**) results. The error bars represent the standard deviation (SD). The values were expressed as mean ± standard error of the mean ($p < 0.05$, $n = 3$).

The post hoc power analysis (power > 0.95) confirms the robustness of these findings, ensuring the observed differences are unlikely due to random variation.

The radical scavenging activity assay, expressed as IC_{50} values (Fig. 9c), further confirmed the superior antioxidant potential of the PM carrier system. The PM carrier system exhibited a significantly lower IC_{50} value (3.98 ± 0.036 mg/mL) compared to *P. oleracea* (4.57 ± 0.012 mg/mL), corresponding to a 12.91% improvement ($p < 0.05$). This reduction in IC_{50} indicates enhanced free radical scavenging activity, suggesting a synergistic effect between phytoconstituents and magnetite, leading to improved antioxidant efficacy. Statistical validation via ANOVA and Dunnett's post hoc test ($p < 0.05$) confirmed the significance of this enhancement. Additionally, the effect size calculations (Cohen's $d = 1.14$, $\eta^2 = 0.64$) indicate a strong effect, reinforcing the superior antioxidant potential of the PM carrier system. A post hoc power analysis (power > 0.95) further validates the statistical robustness of these findings. The superior antioxidant potential of the PM carrier system is likely attributed to the catalytic influence of iron ions, which enhance antioxidant mechanisms such as hydrogen or electron transfer and oxygen discharge. Moreover, the surface electric charge of metallic nanoparticles within the system may contribute to enhanced radical neutralization. Studies indicate that IC_{50} values within the 10–50 mg/mL range correspond to strong antioxidant activity, further confirming the PM carrier system as a potent free radical scavenger[121].

Collectively, these findings demonstrate that the PM carrier system significantly enhances antioxidant properties compared to *P. oleracea* alone, with strong statistical evidence supporting its superior efficacy ($p < 0.001$, large effect size, high statistical power). These results highlight the potential of the PM carrier system as a promising antioxidant platform for various applications.

Cell viability assay

In vitro cytotoxicity assays are commonly employed to assess the effects of various compounds on cell culture models. These assays yield critical data on cell viability, growth, proliferation, and the potential risks associated with the tested substances. Studies have shown that the cytotoxicity of natural products can be influenced by factors such as concentration, duration of exposure, cell culture model, and experimental techniques. Studies have shown that the cytotoxicity of natural products can be influenced by factors such as concentration, duration

of exposure, cell culture model, and experimental techniques. Furthermore, in vitro assays can offer valuable insights for subsequent in vivo studies, especially in drug development[122,123].

Various assays rely on different cell functions to determine cell viability, such as enzyme activity, cell membrane permeability, cell adherence, adenosine triphosphate (ATP) production, co-enzyme production, and nucleotide uptake activity. Among the most used assays are dye exclusion colorimetric, fluorometric, luminometric, and flow cytometric assays. Colorimetric assays are particularly advantageous because they are straightforward, cost-effective, and can be used for both cell suspensions and adherent cells[122,123].

The 3-(4,5-Dimethylthiazol)-diphenyl tetrazolium bromide (MTT) assay is frequently used for high-throughput screening of cell viability in drug toxicity assessment. However, this assay has some limitations. To overcome these limitations, several optimization techniques have been developed. These methods involve the formazan product solubilization using dimethyl sulfoxide, acidified isopropanol, dimethylformamide (DMF), sodium dodecyl sulfate (SDS), or other similar compounds. These techniques also include color stabilization, evaporation prevention, and interference minimization[122–124].

The cytotoxic effects of *P. oleracea* and the PM carrier system were evaluated using an MTT assay on normal human dermal fibroblasts (NHDF), human osteosarcoma cells (HOS), and HeLa cells.

Figure 10a,b summarizes the findings of the test.

Figure 10a,b presents the cytotoxicity results, demonstrating that both *P. oleracea* and the PM carrier system exhibit concentration-dependent cytotoxic effects on cancer cell lines (HOS and HeLa). The most significant cytotoxicity was observed at the highest concentration (200.0 µg/mL), particularly against HeLa and HOS cells. These findings align with previous reports highlighting the antitumor properties of *P. oleracea*[15]. The IC_{50} values corresponding to the herb and PM carrier system are shown in (Table 3).

The MTT assay results demonstrated that NHDF cells maintained high viability at all tested concentrations, with both *P. oleracea* and the PM carrier system exhibiting minimal cytotoxic effects. At 75 µg/mL, NHDF viability remained stable, slightly decreasing from 89.33% (24 h) to 89.19% (72 h). Even at the highest concentration (200 µg/mL), viability declined marginally from 88.52% (24 h) to 88.47% (72 h), confirming negligible toxicity. Similarly, the PM carrier system displayed minimal effects, with NHDF viability ranging from 88.67% (24 h) to 88.16% (72 h) at 75 µg/mL and from 88.22% (24 h) to 87.41% (72 h) at 200 µg/mL.

The high IC_{50} values (> 68 µg/mL) further confirmed the non-toxic nature of both samples toward normal fibroblasts. The slight difference in IC_{50} values (71.19 ± 0.019 µg/mL for *P. oleracea vs.* 68.89 ± 0.15 µg/mL for the PM carrier system) was statistically insignificant ($p > 0.05$). Statistical analysis confirmed no significant differences between the two treatments ($p > 0.05$), supported by a small effect size (Cohen's $d = 0.18$, $\eta^2 = 0.02$), indicating that neither sample significantly impacted NHDF viability. These findings confirm that both *P. oleracea* and the PM carrier system are highly biocompatible with normal cells.

In contrast, the cytotoxic effects on HOS cells were significantly stronger for the PM carrier system. For *P. oleracea*, cell viability decreased from 82.63% (24 h) to 73.55% (72 h) at 75 µg/mL and from 41.88% (24 h) to 34.88% (72 h) at 200 µg/mL. The PM carrier system exhibited enhanced cytotoxicity, reducing viability from 77.63% (24 h) to 70.55% (72 h) at 75 µg/mL and from 37.41% (24 h) to 34.22% (72 h) at 200 µg/mL. At the highest concentration (200 µg/mL), the PM carrier system reduced HOS viability to 34.22% after 72 h, compared to 34.88% for *P. oleracea*, with a statistically significant difference ($p < 0.01$). The IC_{50} values further confirmed the superior cytotoxicity of the PM carrier system (IC_{50} 47.55 ± 0.18 µg/mL) compared to *P. oleracea* (IC_{50} 59.82 ± 0.12 µg/mL), reflecting a 20.50% reduction ($p < 0.001$). The effect size analysis (Cohen's $d = 1.26$, $\eta^2 = 0.62$) indicated a large effect, strongly supporting the impact of the PM carrier system. Moreover, power analysis (> 0.95) confirmed the robustness of these findings, ensuring that the observed differences were not due to random variation. These results demonstrate that the PM carrier system is significantly more cytotoxic to HOS cells than *P. oleracea*, with strong statistical significance ($p < 0.001$) and a large effect size.

HeLa cells were the most sensitive to both treatments, with the PM carrier system exhibiting the most potent cytotoxic effect. At 200 µg/mL, viability decreased to 24.67% after 72 h for the PM carrier system, compared to 30.88% for *P. oleracea*. The IC_{50} values further reinforced the superior effectiveness of the PM carrier system (IC_{50} 44.11 ± 0.11 µg/mL) compared to *P. oleracea* (IC_{50} 55.69 ± 0.02 µg/mL), with a 20.80% reduction ($p < 0.001$). The statistical analysis demonstrated a very large effect size (Cohen's $d = 1.53$, $\eta^2 = 0.74$), confirming the significantly enhanced cytotoxic potential of the PM carrier system. Additionally, power analysis (> 0.95) indicated strong statistical power, reinforcing the reliability of these results. These findings conclusively show that the PM carrier system is significantly more effective than *P. oleracea* in reducing HeLa cell viability, with highly significant statistical differences ($p < 0.001$) and a very large effect size.

Overall, the PM carrier system demonstrated superior anticancer activity against both HOS and HeLa cells compared to *P. oleracea*, while maintaining a high level of biocompatibility with NHDF cells. The statistical analyses, including ANOVA, post hoc tests, effect size calculations, and power analysis, consistently confirmed the significance and robustness of these differences. These findings highlight the superior efficiency of the PM carrier system against cancer cell lines compared to *P. oleracea*, likely due to the combined antitumoral effects of the herb and magnetite. The synergistic interaction between *P. oleracea* and magnetite enhances cytotoxicity against cancer cells while maintaining minimal toxicity to normal cells[15,125]. This effect may be attributed to the higher affinity of cells for iron oxides, which can influence metabolic activity through iron metabolism[126].

Discussion

We successfully developed a novel phytocarrier system (PM carrier system) by integrating *P. oleracea* with magnetite nanoparticles. Raman spectroscopy confirmed the successful intermolecular bond formation between magnetite nanoparticles and *P. oleracea* biomolecules, validating the structural integrity of the PM carrier system. Additionally, XRD analysis revealed characteristic diffraction patterns corresponding to both *P. oleracea* and

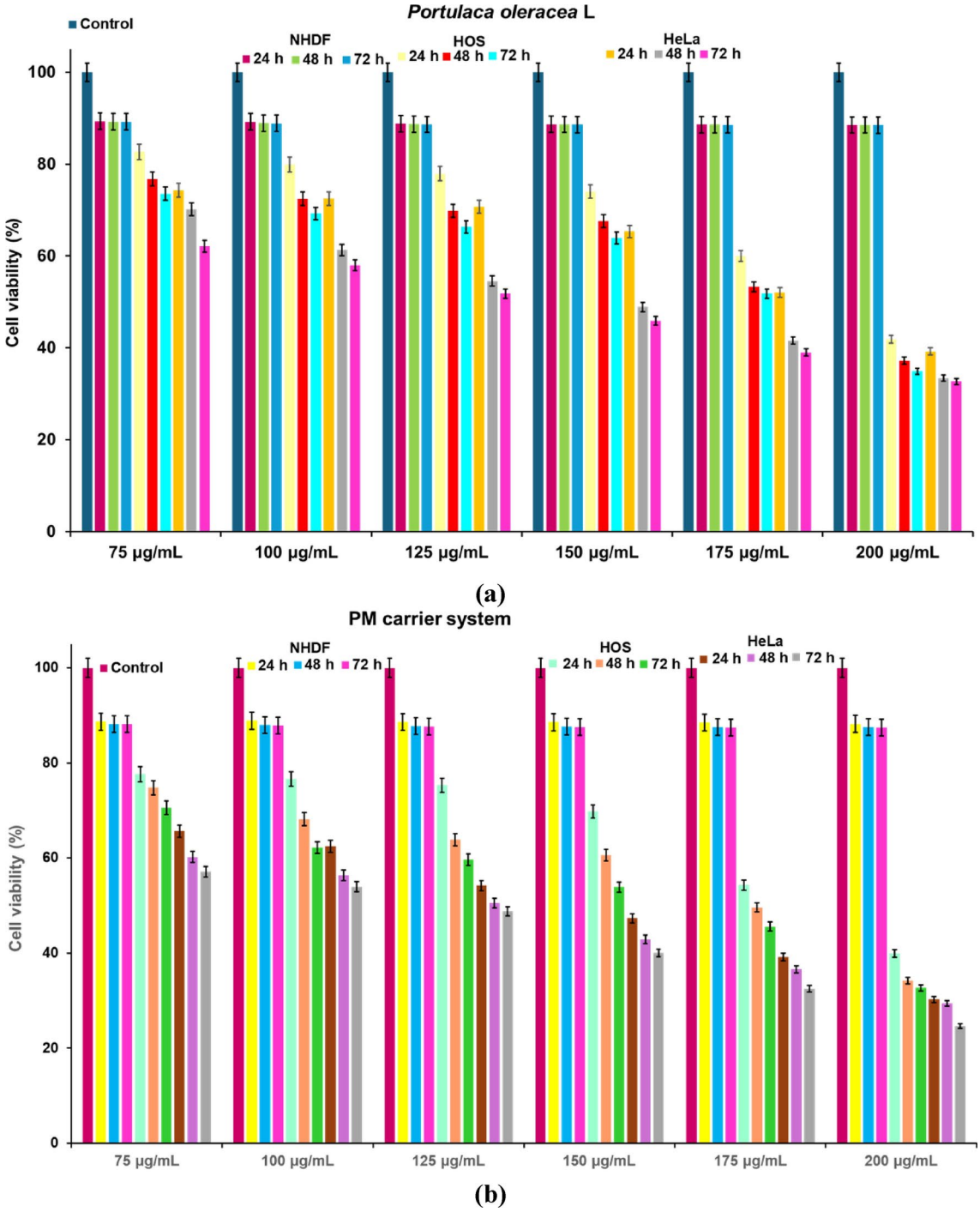

Fig. 10. Viability of NHDF, HOS, and HeLa cells, 24 h after co-incubation with different concentrations of (**a**) *P. oleracea* sample and (**b**) PM carrier system. Positive control wells contained untreated cells, MTT solution, and DMSO. *NHDF* normal human dermal fibroblasts, *HOS* human osteosarcoma cells.

magnetite nanoparticles, further confirming successful incorporation. SEM, EDX, and DLS analyses provided additional structural and morphological evidence supporting the preparation of the PM carrier system.

The structural modifications induced by the integration of magnetite nanoparticles, such as their deposition on the surface and within the pores of herb particles, conferred magnetic properties to the system while enhancing its bioactive profile. Notably, the PM carrier system exhibited a 20.18% increase in total polyphenolic content, a 25.28% higher reducing power, and a 12.91% improvement in antioxidant activity (as indicated by a lower IC_{50} value) compared to *P. oleracea* alone. This enhancement is attributed to the synergistic interaction between phytochemicals and the magnetic component. GC–MS and ESI–QTOF–MS analyses identified 155

Cell lines	Sample	Concentration (µg/mL)	IC_{50} (µg/mL)
NHDF	*P. oleracea*	100.0	71.19 ± 0.019
		125.0	
		150.0	
		175.0	
		200.0	
HOS		100.0	59.82 ± 0.12
		125.0	
		150.0	
		175.0	
		200.0	
HeLa		100.0	55.69 ± 0.02
		125.0	
		150.0	
		175.0	
		200.0	
NHDF	PM carrier system	100.0	68.89 ± 0.15
		125.0	
		150.0	
		175.0	
		200.0	
HOS		100.0	47.55 ± 0.18
		125.0	
		150.0	
		175.0	
		200.0	
HeLa		100.0	44.11 ± 0.11
		125.0	
		150.0	
		175.0	
		200.0	
Control		NA	NA

Table 3. In vitro cytotoxicity of PM carrier system *vs. P. oleracea* as a function of concentration against NHDF, HOS, and HeLa cell lines (after 72 h). Data are represented as mean ± SEM (standard error of the mean) of three independent readings ($n = 3$).

phytoconstituents spanning multiple phytochemical categories, further supporting the enriched bioactivity of the PM carrier system.

Antioxidant screening results suggest that magnetite nanoparticles act as catalysts, facilitating the release of polyphenolic compounds from *P. oleracea*, thereby amplifying its antioxidant potential. Additionally, the surface electric charge of the metallic nanoparticles embedded within the herb matrix may contribute to enhanced radical scavenging activity.

The cytotoxicity of the PM carrier system was evaluated using an MTT assay on normal human dermal fibroblasts (NHDF), human osteosarcoma cells (HOS), and HeLa cells. The findings demonstrated that both *P. oleracea* and the PM carrier system induced dose-dependent reductions in viability in HOS and HeLa cancer cell lines. The enhanced cytotoxicity of the PM carrier system is likely due to the combined effects of bioactive compounds from *P. oleracea* and the influence of iron oxide on cellular metabolic activity. Importantly, both samples exhibited minimal cytotoxic effects on normal NHDF cells, highlighting their biocompatibility.

Collectively, these findings suggest that the PM carrier system holds significant promise for biomedical applications. While this study provides valuable insights into its cytotoxic and antioxidant properties, further research is required to evaluate its bioavailability, in vivo efficacy, and potential for therapeutic applications.

Materials and methods

Reagents and chemicals

All used reagents were analytical grade. Methanol, chloroform, dichloromethane, ethanol, DPPH (2,2-diphenyl-1-picrylhydrazyl), sodium carbonate, gallic acid, acetate buffer solution (pH 4-pH 7), kit ferric reducing antioxidant power (FRAP) assay, were acquired from Sigma Aldrich (München, Germany) and used without further purification. 3-(4,5-Dimethylthiazolyl-2)-2,5-dyphenyltetrazolium bromide (MTT) MTT kit was obtained from AAT Bioquest (Pleasanton, California). Ultrapure water was used in all experiments.

Cell lines

Normal human dermal fibroblasts (NHDF), MG-63 human osteosarcoma (HOS), and HeLa cell lines were purchased from the American Type Culture Collection (ATCC; Manassas, VA, USA).

Each cellular line was cultivated at 37 °C, in the next culture media: Dulbecco's Modified Eagle's Medium (Gibco, Life Technologies, Leicestershire, UK), supplemented with 10% fetal bovine serum (FBS), and 1% antibiotic–antimycotic solution (Sigma Aldrich).

Plant material

P. oleracea samples were collected in July 2022 from the area of Timiş County, Romania (geographic coordinates 45°43′02" N and 21°19′31" E). The formal identification of the plant material used in our study has been undertaken by Dr Cornelia Bejenaru from the Department of Pharmaceutical Botany and by Dr Ludovic-Everard Bejenaru from the Department of Pharmacognosy & Phytotherapy, Faculty of Pharmacy, University of Medicine and Pharmacy of Craiova, Romania. Voucher specimens (PORT-OLR-2022–0307) were deposited at the Department of Pharmaceutical Botany, Faculty of Pharmacy, University of Medicine and Pharmacy of Craiova.

Magnetite sample

Magnetite sample was offered by the national research& development institute for non-ferrous and rare metals and was prepared according to a procedure described in our previous paper[126].

Phytocarrier system components preparation

The freeze-dried plant samples (whole plant) were grounded using a planetary Fritsch Pulverisette mill (Idar-Oberstein, Germany) (650 rpm for 8 min at 23 °C), then sieved through ASTM sieves. Only particles ranging from 0.25 ÷ 0.30 mm were used in this study. The plant samples were subject to sonication extraction (Elmasonic, Singen, Germany) for 45 min at 40 °C and 60 Hz dissolved in methanol (15 mL), All experiments were prepared in triplicate.

GC–MS analysis

Gas chromatography was carried out on the GC–MS QP2020NX Shimadzu apparatus with a ZB-5MS capillary column (30 m × 0.25 mm i.d. × 0.25 µm) (Agilent Technologies, Santa Clara, CA, USA), helium, flow of 1 mL/min.

GC–MS separation conditions

The oven temperature program started from 50 °C (hold for 2 min) to 300 °C (rate of 5 °C/min, kept for 4 min). The temperature of the injector was 280 °C, and the temperature at the interface was 225 °C. The compounds' mass was registered at 70 eV ionization energy, starting after 2 min of solvent delay. The mass spectrometer source was heated at 230 °C, and the MS Quad at 160 °C. Compounds were identified based on their mass spectra, compared to the NIST 0.2 mass spectra library database (USA National Institute of Science and Technology software, (NIST, Gaithersburg, MD, USA), and literature review.

Mass spectrometry

MS experiments were performed on an EIS–QTOF–MS analysis (Bruker Daltonics, Bremen, Germany). The mass spectra were acquired in the positive ion mode in a mass range of 100–3000 m/*z*, scan speed was 2.0 scans/s, 25–85 eV collision energy, and the source block temperature was 80 °C. The identification of phytoconstituents was based on standard library NIST/NBS-3 (national institute of standards and technology/national bureau of standards) (NIST, Gaithersburg, MD, USA). The obtained mass spectra values and the identified secondary metabolites are presented in (Table 1S).

Phytocarrier system preparation (PM carrier system)

To prepare the PM carrier system, *P. oleracea* (freeze-drying herb) and magnetite were mixed (1:3 mass ratio), and then milled in a planetary mill (Fritsch Pulverisette mill) for 15 min. Each experiment was repeated three times.

Characterization of the phytocarrier system

FTIR spectroscopy

Data collections were conducted after 25 recordings at a resolution of 4 cm^{-1}, in the range of 4000–400 cm^{-1} on Shimadzu AIM-9000 with ATR devices (Shimadzu, Japan).

Raman spectroscopy

Raman investigations were performed on LabRam Soleil Horiba (Confocal Raman Microscope)-Raman SuperHead Horiba coupled with DSC3 + Mettler Toledo.

XDR spectroscopy

The X-ray powder diffraction (XRD) was carried out on a Bruker AXS D8-Advance X-ray diffractometer (*Bruker AXS* GmbH, Karlsruhe, Germany) (CuKα radiation, $k = 0.1541$ nm) equipped with a rotating sample stage, Anton Paar TTK low-temperature cell (−180 °C ÷ 450 °C), high vacuum, inert atmosphere, and relative humidity control, Anton Paar TTK high- temperature cell (up to 1600 °C). The XRD patterns were compared with those from the ICDD Powder Diffraction Database (ICDD file No. 04-015-9120). The average crystallite size and the phase content were determined using the whole-pattern profile-fitting method (WPPF).

SEM analysis
SEM micrographs were obtained with an SEM–EDS system (QUANTA INSPECT F50) equipped with a field-emission gun (FEG), 1.2 nm resolution, and energy dispersive X-ray spectrometer (EDS) with an MnK resolution of 133 eV.

Dynamic light scattering (DLS) particle size distribution analysis
DLS analysis was conducted on a Microtrac/Nanotrac 252 (Montgomeryville, PA, USA). Each sample was analyzed in triplicate at room temperature (22 °C) at a scattering angle of 172°.

Magnetic properties
Magnetic characterizations of the PM carrier system were measured using a vibrating sample magnetometer (type VSM 880—ADE Technologies, USA), at room temperature (22 °C), in the range of values of the magnetizing field, 0–950 kA/m. The frequency dependence of the samples was determined according to Eq. (1):

$$\mu\,(\mathrm{f})\neg = \ \mu'\neg\,(\mathrm{f}) - \mathrm{i}\mu''\neg\,(\mathrm{f}) \tag{1}$$

The measurements were carried out on an Agilent LCR-meter (E-4980A type), at 22 °C, over the frequency range (1 kHz to 2 MHz) in conjunction with a coil containing a vial as sample holder.

Antioxidant activity
The antioxidant activity of the PM carrier system was estimated using three different assays: TPC (Folin–Ciocalteu), DPPH radical scavenging and FRAP assays.

The PM carrier system (0.20 g) and *P. oleracea* (0.20 g) samples were dissolved in 5 mL ethanol (70%). The mixtures were stirred at room temperature (22 °C) for eight hours, then centrifuged at 5000 rpm for 10 min. The supernatant was then collected for use in the TPC (Folin–Ciocalteu), DPPH and FRAP assays.

Determination of TPC
The TPC in the PM carrier system and *P. oleracea* samples was determined spectrophotometrically (BMGLabtech, FLUOstar OPTIMA, Offenburg, Germany) according to the Folin–Ciocalteu procedure adapted from our earlier publication[127].

The results are expressed in gallic acid equivalents (mg GAE/g sample). Sample concentrations were calculated based on the linear equation obtained from the standard curve ($y = 0.0019x + 0.1627$) and the correlation coefficient (R^2 0.9998).

DPPH radical scavenging assay
Radical scavenging properties of the PM carrier system and the *P. oleracea* samples were carried out according to the procedure described in our earlier publication[127].

All analyses were carried out in triplicates, and absorbance was recorded at 520 nm (BMGLabtech, FLUOstar OPTIMA, Offenburg, Germany).

The half-maximal inhibitory concentration (IC_{50}) values (µg/mL). were obtained from the inhibition percentage (Inh%), determined according to Eq. (2), from the equation from the calibration curve generated for each sample:

$$\mathrm{Inh}\% = (\mathrm{A}_0 - \ \mathrm{A}_1)\,/\mathrm{A}_0 \times 10 \tag{2}$$

All experiments for antioxidant activity screening were performed in triplicate.

FRAP assay
The ferric reducing/antioxidant activity of the sample was determined spectrophotometrically using a FRAP Assay Kit (MAK369-1KT, Sigma-Aldrich). The absorbance was measured at 595 nm using a UV–Vis spectrometer (BMGLabtech, FLUOstar Optima, Offenburg, Germany). The results were expressed in mM Fe^{2+}, calculated according to Eq. (3):

$$\frac{nmolFe^{2+}xF_D}{V} \tag{3}$$

where: nmol Fe^{2+}—the iron ions (Fe^{2+}) amount generated from the calibration curve of each sample; F_D—the dilution factor; V—volume of each sample (µL).

Cell culture procedure

The target cell lines used in this study included normal human dermal fibroblasts (NHDF), MG-63 human osteosarcoma (HOS), and HeLa cervical cancer cells, all of which were purchased from the American Type Culture Collection (ATCC; Manassas, VA, USA).

Cells were maintained under standard culture conditions at 37 °C in a humidified incubator with 5% CO_2. The Dulbecco's Modified Eagle's Medium (DMEM; Gibco, Life Technologies, Leicestershire, UK) was used as the culture medium, supplemented with 10% FBS and 1% antibiotic–antimycotic solution (Sigma-Aldrich, St. Louis, MO, USA). For the experiment, cells were seeded in 96-well plates at a density of 4×10^3 cells per well and allowed to adhere for six hours, after which the culture medium was replaced with fresh medium containing

various concentrations (100, 125, 150, 175, and 200 µg/mL) of *P. oleracea* and the PM carrier system, dissolved in the culture medium. Cells were then incubated for 24 to 72 h[128].

For the control group, the medium was aspirated and replaced with fresh standard culture medium without treatment. Positive and negative controls were included, with each condition tested in eight wells per test material.

All experiments were conducted in triplicate to ensure reproducibility. Following incubation for 24, 48, and 72 h, cell viability was assessed using the MTT assay.

MTT assay

To assess cell viability, the culture medium was aspirated from each well, and 25 µL of MTT reagent was added to each well. The plates were then incubated at 37 °C in a CO_2 incubator for 24, 48, and 72 h[128].

Following incubation, the formazan crystals formed by metabolically active cells were dissolved by adding dimethyl sulfoxide (DMSO, 100 µL per well). The absorbance of the resulting solution was measured at 540 nm using a Multi-Mode Microplate Reader (Synergy HTX, BioTek, Winooski, VT, USA).

The cell viability (%) was determined according to Eq. (4):

$$\mathrm{CV}\ (\%) = 100 \times \frac{\mathrm{OD_{Sample}} - \mathrm{OD_{blank}}}{\mathrm{OD_{Control}} - \mathrm{OD_{blank}}} \tag{4}$$

where CV (%)—the cellular viability; OD—the optical density of the wells containing: (a) cells with the evaluated sample (OD sample), (b) only cells (OD control), and (c) cell culture media without cells (OD blank).

According to the manufacturer's specifications, the positive control consisted of untreated cells incubated with MTT and DMSO, while the negative control contained only dead cells incubated with MTT and DMSO.

The IC_{50} values were determined as the concentration of *P. oleracea* and the PM carrier systems at which 50% of the cells remained viable for NHDF, HOS, and HeLa cell lines. Cell viability was plotted as a function of concentration, and IC_{50} values were calculated using nonlinear regression analysis[129,130].

All experiments were performed in triplicate to ensure statistical reliability and reproducibility.

Statistical analysis

All experiments were performed in triplicate for all samples, all calibration curves, and concentrations. Statistical analysis was carried out using Student's *t*-test, and expressed as mean ± SD, using Microsoft Office Excel 2019 (Microsoft Corporation, Redmond, WA, USA). Dunnett's multiple comparison post hoc test following a one-way ANOVA test was used to analyze the results. *P*-values < 0.05 were considered statistically significant.

Conclusions

This study successfully demonstrates the development of a novel phytocarrier system (PM carrier system), which integrates magnetite nanoparticles into *P. oleracea*. Comprehensive characterization through FTIR, Raman spectroscopy, XRD, DLS, and SEM–EDX confirms the successful formation of the PM carrier system, validating the structural and physicochemical interactions between the plant-derived biomolecules and the magnetic nanoparticles. The magnetic properties of the PM carrier system were also thoroughly evaluated, further supporting its functional potential.

The results reveal that the PM carrier system significantly enhances biological properties when compared to *P. oleracea* alone, particularly in terms of antioxidant potential and in vitro cytotoxicity against two cancer cell lines, HOS and HeLa. Statistical analysis of TPC, DPPH radical scavenging activity and FRAP assay (expressed as IC_{50}) shows a marked increase in antioxidant activity, suggesting that the incorporation of magnetite enhances the bioavailability and efficacy of polyphenolic compounds. Furthermore, MTT assay results indicate a dose-dependent cytotoxic effect on HOS and HeLa cancer cells, with significantly lower IC_{50} values, while demonstrating high biocompatibility with normal NHDF cells. These findings strongly suggest a synergistic effect between the phytoconstituents and the magnetic component, resulting in enhanced therapeutic efficacy.

The PM carrier system showcases integrated magnetic properties, a stable micro-to-nanoscale structure, and enhanced biological activity, making it a promising candidate for biomedical applications. Its ability to improve bioavailability, amplify antioxidant activity, and selectively target cancer cells positions it as a versatile platform with potential for various applications. Future studies should focus on in vivo investigations to further confirm its therapeutic potential, underscoring its promise as a novel candidate for biomedical use.

Patents

A patent application was submitted to the Romanian State Office for Inventions and Trademarks.

Data availability

All data generated or analysed during this study are included in this published article and its supplementary information files.

Received: 16 August 2024; Accepted: 27 February 2025
Published online: 13 March 2025

References

1. ***Flora RPR, III (Ed. Academiei RPR, București, 1955).
2. Srivastava, R., Srivastava, V. & Singh, A. Multipurpose benefits of an underexplored species purslane (*Portulaca oleracea* L.): A critical review. *Environ. Manag.* https://doi.org/10.1007/s00267-021-01456-z (2021).
3. Tutin, T. G. et al. Psilotaceae to platanaceae. In *Flora Europaea* (eds Tutin, T. G. et al.) (Cambridge University Press, 1996).

4. Wang, M. et al. Extraction, purification, structural characteristics, biological activity and application of polysaccharides from *Portulaca oleracea* L. (Purslane): A review. *Molecules* **28**, 4813. https://doi.org/10.3390/molecules28124813 (2023).
5. Nyffeler, R. & Eggli, U. Disintegrating *Portulacaceae*: A new familial classification of the suborder *Portulacineae* (*Caryophyllales*) based on molecular and morphological data. *Taxon* **59**, 227–240 (2010).
6. Ocampo, G. & Columbus, J. T. Molecular phylogenetics, historical biogeography, and chromosome number evolution of Portulaca (Portulacaceae). *Mol. Phylogenet. Evol.* **63**, 97–112 (2012).
7. Kumar, A. et al. A review on bioactive phytochemicals, ethnomedicinal and pharmacological importance of purslane (*Portulaca oleracea* L.). *Heliyon* **8**, e08669. https://doi.org/10.1016/j.heliyon.2021.e08669 (2021).
8. Pârvu, C. *Universul Plantelor* (Editura ASAB, 2006).
9. Tran, T. T., Bui, P. H., Phan, N. T. T. & My, D. H. Bioactive compounds from *Portulaca oleracea* L. extract. *Chem. Eng. Trans.* **106**, 637–642 (2023).
10. Segneanu, A. E. et al. Therapeutic use of some Romanian medicinal plants. In *Pharmacognosy—Medicinal Plants* (eds Perveen, S. & Al-Taweel, A.) (IntechOpen, 2019).
11. Rahimi, V. B., Ajam, F., Rakhshandeh, H. & Askari, V. R. A pharmacological review on *Portulaca oleracea* L.: focusing on anti-inflammatory, antioxidant, immunomodulatory and antitumor activities. *J. Pharmacopunct.* **22**, 7–15 (2019).
12. Zhou, Y. X. et al. *Portulaca oleracea* L.: A review of phytochemistry and pharmacological effects. *Biomed. Res. Int* **2015**, 925631. https://doi.org/10.1155/2015/925631 (2015).
13. Petran, M., Dragos, D. & Gilca, M. Historical ethnobotanical review of medicinal plants used to treat children diseases in Romania (1860s–1970s). *J. Ethnobiol. Ethnomed.* **16**, 15. https://doi.org/10.1186/s13002-020-00364-6 (2020).
14. Fukalova, T. K., García-Martínez, M. D. & Raigón, M. D. Nutritional composition, bioactive compounds, and volatiles profile characterization of two edible undervalued plants: *Portulaca oleracea* L. and *Porophyllum ruderale* (Jacq.) cass. *Plants* **11**, 377. https://doi.org/10.3390/plants11030377 (2022).
15. Shao, G. et al. Therapeutic potential of traditional Chinese medicine in the prevention and treatment of digestive inflammatory cancer transformation: *Portulaca oleracea* L. as a promising drug. *J. Ethnopharmacol.* **327**, 117999. https://doi.org/10.1016/j.jep.2024.117999 (2024).
16. Zhao, R., Zhang, T., Ma, B. & Li, X. Antitumor activity of *Portulaca oleracea* L. polysaccharide on HeLa cells through inducing TLR4/NF-κB signaling. *Nutr. Cancer* **69**, 131–139 (2016).
17. Jia, G. et al. Anti-cervical cancer activity of *Portulaca oleracea* L. and the mechanism of synergistic cisplatin. *J. Funct. Foods* **98**, 105267. https://doi.org/10.1016/j.jff.2022.105267 (2022).
18. Truc, T. T., Bui, P. H., Phan, N. T. T., My, D. H. & Minh, T. N. K. Bioactive compounds from *Portulaca oleracea* L. extract. *Chem. Eng. Trans.* **106**, 637–642 (2023).
19. Fu, Q. et al. *Portulaca oleracea* polysaccharides modulate intestinal microflora in aged rats in vitro. *Front. Microbiol.* **13**, 841397. https://doi.org/10.3389/fmicb.2022.841397 (2022).
20. Liu, Z. T. et al. Optimization of ultrasound-assisted extraction of flavonoids from *Portulaca oleracea* L., the extraction kinetics and bioactivity of the extract. *J. Appl. Res. Med. Aromat. Plants* **37**, 100512. https://doi.org/10.1016/j.jarmap.2023.100512 (2023).
21. Isah, T. Stress and defense responses in plant secondary metabolites production. *Biol. Res.* **52**, 39 (2019).
22. Yang, L. et al. Response of plant secondary metabolites to environmental factors. *Molecules* **23**, 762 (2018).
23. Segneanu, A. E., Zuguang, Y., Dabici, A., Jianrong, L. & Grozescu, I. Comparative analytical study of active compounds from zingiber officinale. *Optoelectron. Adv. Mater.* **6**, 652–655 (2012).
24. Segneanu, A. E., Grozescu, I. & Sfirloaga, P. The influence of extraction process parameters of some biomaterials precursors from Helianthus annuus. *Dig. J. Nanomater. Biostruct.* **8**, 1423–1433 (2013).
25. Segneanu, A. E., Damian, D., Hulka, I., Grozescu, I. & Salifoglou, A. A simple and rapid method for calixarene-based selective extraction of bioactive molecules from natural products. *Amino Acids* **4**, 849–858 (2016).
26. Ahmad, R., Srivastava, S., Ghosh, S. & Khare, S. K. Phytochemical delivery through nanocarriers: A review. *Coll. Surf. B Biointerfaces* **197**, 111389. https://doi.org/10.1016/j.colsurfb.2020.111389 (2021).
27. Singh, I. P., Ahmad, F., Chatterjee, D., Bajpai, R. & Sengar, N. Natural products: Drug discovery and development. In *Drug Discovery and Development from Targets and Molecules to Medicines* (ed. Poduri, R.) (Springer Nature, 2021).
28. Hkiri, K., Elsayed, H., Mohamed, A., Ghotekar, S. & Maaza, M. Green synthesis of cerium oxide nanoparticles using *Portulaca oleracea* extract: photocatalytic activities. *Inorg. Chem. Commun.* **162**, 112243. https://doi.org/10.1016/j.inoche.2024.112243 (2024).
29. Abdel-Rahman, M. A. et al. Exploring the antimicrobial, antioxidant, and antiviral potential of eco-friendly synthesized silver nanoparticles using leaf aqueous extract of *Portulaca oleracea* L.. *Pharmaceuticals* **17**, 317. https://doi.org/10.3390/ph17030317 (2024).
30. Mohammadi, M. & Pourseyed Aghaei, F. Magnetite Fe_3O_4 surface as an effective drug delivery system for cancer treatment drugs: density functional theory study. *J. Biomol. Struct. Dyn.* **39**, 2798–2805 (2021).
31. Gómez-Sotomayor, R., Ahualli, S., Viota, J. L., Rudzka, K. & Delgado, Á. V. Iron/magnetite nano-particles as magnetic delivery systems for antitumor drugs. *J. Nanosci. Nanotechnol.* **15**, 3507–3514 (2015).
32. Włodarczyk, A., Gorgoń, S., Radoń, A. & Bajdak-Rusinek, K. Magnetite nanoparticles in magnetic hyperthermia and cancer therapies: challenges and perspectives. *Nanomaterials* **12**, 1807. https://doi.org/10.3390/nano12111807 (2022).
33. Chavda, V. P. et al. Nano-drug delivery systems entrapping natural bioactive compounds for cancer: Recent progress and future challenges. *Front. Oncol.* **12**, 867655. https://doi.org/10.3389/fonc.2022.867655 (2022).
34. Segneanu, A. E., Vlazan, P., Svera, P., Grozescu, I. & Sfirloaga, P. Magnetic cobalt ferrite nanoparticles: synthesis and surface functionalization with naturally small peptide. *Digest. J. Nanomater. Biostruct.* **9**, 891–898 (2014).
35. Socoliuc, V. et al. Magnetic nanoparticle systems for nanomedicine—A science perspective. *Magnetochemistry* **6**, 2. https://doi.org/10.3390/magnetochemistry6010002 (2020).
36. Comanescu, C. Magnetic nanoparticles: Current advances in nanomedicine, drug delivery, and MRI. *Chemistry* **4**, 872–930 (2022).
37. Emran, T. B. et al. Multidrug resistance in cancer: Understanding molecular mechanisms, immunoprevention, and therapeutic approaches. *Front. Oncol.* **12**, 2581. https://doi.org/10.3389/fonc.2022.891652 (2022).
38. Stroescu, M., Stoica-Guzun, A., Ghergu, S., Chira, N. & Jipa, I. Optimization of fatty acids extraction from *Portulaca oleracea* seed using response surface methodology. *Ind. Crops Prod.* **43**, 405–411 (2013).
39. Pasca, M. B., Pallag, A., Tit, D. M., Magyar, I. & Gitea, D. Comparative study of flavones content in different extracts obtained from *Portulaca oleracea* L.. *Analele Univ. Oradea Fascicula* **XIV**, 404–410 (2015).
40. Anghel, A., Ilie, I. M., Olaru, O. T., Dinu, M. & Ancuceanu, R. V. HPTLC qualitative and quantitative detection of sterols in species of the *Portulaca* genus from Romania. *Farmacia* **63**, 696–699 (2015).
41. Činčala, Ľ, Illeová, V., Antosova, M., Štefuca, V. & Polakovič, M. Investigation of plant sources of hydroperoxide lyase for 2(E)-hexenal production. *Acta Chim. Slovaca* **8**, 156–165 (2015).
42. Kazemifard, A. G., Moore, D. E. & Mohammadi, A. Capillary gas chromatography determination of benzaldehyde arising from benzyl alcohol used as preservative in injectable formulations. *J. Pharm. Biomed. Anal.* **31**, 685–691 (2003).
43. Gajić, I. et al. The chemical composition of the essential oil and volatile compounds from caraway fruit (*Carum carvi* L.) extracted by headspace-solid phase microextraction and the antioxidant activity. *Adv. Technol.* **9**, 37–43 (2020).

44. Chen, Q. et al. Preparative isolation and purification of cuminaldehyde and p-menta-1,4-dien-7-al from the essential oil of *Cuminum cyminum* L. by high-speed counter-current chromatography. *Anal. Chim. Acta* **689**, 149–154 (2011).
45. Segneanu, A. E. et al. Romanian wild-growing *Chelidonium majus*—An emerging approach to a potential antimicrobial engineering carrier system based on AuNPs: in vitro investigation and evaluation. *Plants* **13**, 734. https://doi.org/10.3390/plants13050734 (2024).
46. Moretto, J. A. S. et al. Effects of different cultivation conditions on the production of β-cyclocitral and β-ionone in *Microcystis aeruginosa*. *BMC Microbiol.* **22**, 78. https://doi.org/10.1186/s12866-022-02473-6 (2022).
47. Segneanu, A. E. et al. Chemical screening of metabolites profile from Romanian *Tuber* spp.. *Plants (Basel)* **10**, 540. https://doi.org/10.3390/plants10030540 (2021).
48. Petropoulos, S. A. et al. Nutritional value, chemical composition and cytotoxic properties of common purslane (*Portulaca oleracea* L.) in relation to harvesting stage and plant part. *Antioxidants (Basel)* **8**, 293. https://doi.org/10.3390/antiox8080293 (2019).
49. Al-Quwaie, D. A. et al. Characterization of *Portulaca oleracea* whole plant: evaluating antioxidant, anticancer, antibacterial, and antiviral activities, and application as a quality enhancer in yogurt. *Molecules* **28**, 5859. https://doi.org/10.3390/molecules28155859 (2023).
50. Ning, K. et al. Protective effects of different molecular weights of purslane (*Portulaca oleracea* L.) aqueous extract on DSS-induced ulcerative colitis in mice. *Antioxidants* **12**, 1400. https://doi.org/10.3390/antiox12071400 (2023).
51. Zhou, Y. X. et al. *Portulaca oleracea* L.: a review of phytochemistry and pharmacological effects. *BioMed Res. Int.* **1**, 925631. https://doi.org/10.1155/2015/925631 (2015).
52. Kumar, A., Sreedharan, S., Kashyap, A. K., Singh, P. & Ramchiary, N. A review on bioactive phytochemicals and ethnopharmacological potential of purslane (*Portulaca oleracea* L.). *Heliyon* **8**, e08669. https://doi.org/10.1016/j.heliyon.2021.e08669 (2021).
53. Chugh, V., Mishra, V., Dwivedi, S. V. & Sharma, K. D. Purslane (*Portulaca oleracea* L.): An underutilized wonder plant with potential pharmacological value. *Pharm. Innov. J.* **8**, 236–246 (2019).
54. Lei, X., Li, J., Liu, B., Zhang, N. & Liu, H. Separation and identification of four new compounds with antibacterial activity from *Portulaca oleracea* L.. *Molecules* **20**, 16375–16387 (2015).
55. Hou, J. et al. An integrative pharmacology-based approach for evaluating the potential effects of purslane seed in diabetes mellitus treatment using UHPLC-LTQ-Orbitrap and TCMIP V2.0. *Front. Pharmacol.* **11**, 593693. https://doi.org/10.3389/fphar.2020.593693 (2021).
56. He, X. et al. Deciphering the effective constituents and mechanisms of *Portulaca oleracea* L. for treating NASH via integrating bioinformatics analysis and experimental pharmacology. *Front. Pharmacol.* **12**, 818227. https://doi.org/10.3389/fphar.2021.818227 (2022).
57. Yang, X., Ying, Z., Liu, H., Ying, X. & Yang, G. A new homoisoflavone from *Portulaca oleracea* L. and its antioxidant activity. *Nat. Prod. Res.* **32**, 1–7 (2018).
58. Nemzer, B., Al-Taher, F. & Abshiru, N. Phytochemical composition and nutritional value of different plant parts in two cultivated and wild purslane (*Portulaca oleracea* L.) genotypes. *Food Chem.* **308**, 126621. https://doi.org/10.1016/j.foodchem.2020.126621 (2020).
59. Rahimi, V. B., Ajam, F., Rakhshandeh, H. & Askari, V. R. A pharmacological review on *Portulaca oleracea* L.: focusing on anti-inflammatory, antioxidant, immunomodulatory, and antitumor activities. *J. Pharmacopunct.* **22**, 7–15 (2019).
60. Qi, J. et al. Development status of chemical constituents and pharmacological effects of *Portulaca oleracea* L.. *Highlights Sci. Eng. Technol.* **2**, 243–252 (2022).
61. Naeem, F. & Khan, S. H. Purslane (*Portulaca oleracea* L.) as a phytogenic substance—A review. *J. Herbs. Spices Med. Plants* **19**, 216–232 (2013).
62. Baradaran Rahimi, V. et al. Anti-inflammatory and anti-oxidant activity of *Portulaca oleracea* extract on LPS-induced rat lung injury. *Molecules* **24**, 139. https://doi.org/10.3390/molecules24010139 (2019).
63. Fernández-Poyatos, M. D. P., Llorent-Martínez, E. J. & Ruiz-Medina, A. Phytochemical composition and antioxidant activity of *Portulaca oleracea*: influence of the steaming cooking process. *Foods* **10**, 94. https://doi.org/10.3390/foods10010094 (2021).
64. Khalil, W. A. et al. Ethanolic purslane (*Portulaca oleracea*) leaf extract improves the quality of cryopreserved goat semen. *Andrologia* **2023**, 7771525. https://doi.org/10.1155/2023/7771525 (2023).
65. Balabanova, V. et al. Bioinformatic insight into *Portulaca oleracea* L. (Purslane) of Bulgarian and Greek origin. *Acta Biol. Cracov. Ser. Bot.* **62**, 7–21 (2020).
66. Li, K. et al. A review on ethnopharmacology, phytochemistry, pharmacology, and potential uses of *Portulaca oleracea* L. *J. Ethnopharmacol.* **319**, 117211. https://doi.org/10.1016/j.jep.2023.117211 (2024).
67. Chang, S. et al. Amino acid sequences characterization and anti-inflammatory potency evaluation of *Portulaca oleracea* L. oligopeptides in macrophages. *RSC Adv.* **10**, 7321–7327 (2020).
68. Gu, C., Mao, X., Chen, D., Yu, B. & Yang, Q. Isoleucine plays an important role in maintaining immune function. *Curr. Protein Pept. Sci.* **20**, 644–651 (2019).
69. Dhama, K. et al. Medicinal and therapeutic potential of herbs and plant metabolites/extracts countering viral pathogens—Current knowledge and future prospects. *Curr. Drug Metab.* **19**, 236–263 (2018).
70. Kim, S. H., Roszik, J., Grimm, E. A. & Ekmekcioglu, S. Impact of L-arginine metabolism on immune response and anticancer immunotherapy. *Front. Oncol.* **8**, 67. https://doi.org/10.3389/fonc.2018.00067 (2018).
71. Chiangjong, W., Chutipongtanate, S. & Hongeng, S. Anticancer peptide: physicochemical property, functional aspect, and trend in clinical application (review). *Int. J. Oncol.* **57**, 678–696 (2020).
72. Lieu, E. L., Nguyen, T., Rhyne, S. & Kim, J. Amino acids in cancer. *Exp. Mol. Med.* **52**, 15–30 (2020).
73. Albaugh, V. L., Pinzon-Guzman, C. & Barbul, A. Arginine metabolism and cancer. *Surg. Oncol.* **115**, 273–280 (2017).
74. Wei, Z., Liu, X., Cheng, C., Yu, W. & Yi, P. Metabolism of amino acids in cancer. *Front. Cell Dev. Biol.* **8**, 603837. https://doi.org/10.3389/fcell.2020.603837 (2021).
75. Yang, J. et al. Regulation of ferroptosis by amino acid metabolism in cancer. *Int. J. Biol. Sci.* **18**, 1695–1705 (2022).
76. Pant, A. & Yang, Z. Asparagine: an achilles heel of virus replication?. *ACS Infect. Dis.* **6**, 2301–2303 (2020).
77. Liang, H. et al. Methionine played a positive role in improving the intestinal digestion capacity, anti-inflammatory reaction, and oxidation resistance of grass carp, *Ctenopharyngodon idella*, fry. *Fish Shellfish Immunol.* **128**, 389–397 (2022).
78. Melano, I. et al. Effects of basic amino acids and their derivatives on SARS-CoV-2 and influenza A virus infection. *Viruses* **13**, 7. https://doi.org/10.3390/v13071301 (2021).
79. Aiyelabola, T. et al. Synthesis, characterization, and antimicrobial activities of coordination compounds of aspartic acid. *J. Chem.* **2016**, 7317015. https://doi.org/10.1155/2016/7317015 (2016).
80. Ji, Y., Hou, Y. & Blachier, F. Editorial: Amino acids in intestinal growth and health. *Front. Nutr.* **10**, 1172548. https://doi.org/10.3389/fnut.2023.1172548 (2023).
81. Mani, S. et al. The updated review on plant peptides and their applications in human health. *Int. J. Pept. Res. Ther.* **28**, 135. https://doi.org/10.1007/s10989-022-10437-7 (2022).
82. He, M. & Ding, N. Plant unsaturated fatty acids: multiple roles in stress response. *Front. Plant Sci.* **11**, 562785. https://doi.org/10.3389/fpls.2020.562785 (2020).
83. Coniglio, S., Shumskaya, M. & Vassiliou, E. Unsaturated fatty acids and their immunomodulatory properties. *Biology* **12**, 279. https://doi.org/10.3390/biology12020279 (2023).

84. Liga, S., Paul, C. & Péter, F. Flavonoids: overview of biosynthesis, biological activity, and current extraction techniques. *Plants* **12**, 2732. https://doi.org/10.3390/plants12142732 (2023).
85. Ullah, A. et al. Important flavonoids and their role as a therapeutic agent. *Molecules* **25**, 5243. https://doi.org/10.3390/molecules25225243 (2020).
86. Aryal, B. et al. Potential therapeutic applications of plant-derived alkaloids against inflammatory and neurodegenerative diseases. *Evid. Based Complement. Alternat. Med.* https://doi.org/10.1155/2022/7299778 (2022).
87. Franco, R., Reyes-Resina, I. & Navarro, G. Dopamine in health and disease: much more than a neurotransmitter. *Biomedicines* **9**, 109. https://doi.org/10.3390/biomedicines9020109 (2021).
88. Dash, D. K., Tyagi, C. K., Sahu, A. K. & Tripathi, V. Revisiting the medicinal value of terpenes and terpenoids. In *Revisiting Plant Biostimulants* (ed. Meena, V.) (IntechOpen, 2022).
89. Zhang, Y. et al. A brief review of phenolic compounds identified from plants: their extraction, analysis, and biological activity. *Nat. Prod. Commun.* **17**, 1–14 (2022).
90. Gao, X. Y. et al. Scopoletin: a review of its pharmacology, pharmacokinetics, and toxicity. *Front. Pharmacol.* **15**, 1268464. https://doi.org/10.3389/fphar.2024.1268464 (2024).
91. Vezza, T. et al. Phytosterols: nutritional health players in the management of obesity and its related disorders. *Antioxidants* **9**, 1266. https://doi.org/10.3390/antiox9121266 (2020).
92. Razna, K. et al. Biological functions of lignans in plants. *Agric. (Ponohospodárstvo)* **67**, 155–165 (2021).
93. Segneanu, A. et al. Bioactive molecules profile from natural compounds. In *Amino Acid—New Insights and Roles in Plant and Animal* (eds Asao, T. & Asaduzzaman, M.) (IntechOpen, 2017).
94. Segneanu, A. E. et al. An innovative approach to a potential neuroprotective *Sideritis scardica*-clinoptilolite phyto-nanocarrier: *in vitro* investigation and evaluation. *Int. J. Mol. Sci.* **25**, 1712. https://doi.org/10.3390/ijms25031712 (2024).
95. Bensemmane, N. et al. Quantification of phenolic acids by partial least squares fourier-transform infrared (PLS-FTIR) in extracts of medicinal plants. *Phytochem. Anal.* **32**, 206–221 (2021).
96. Pang, M., Jiang, S., Cao, L. & Pan, L. Novel synthesis of steryl esters from phytosterols and amino acid. *J. Agric. Food Chem.* **59**, 10732–10736 (2011).
97. Chyau, C. et al. *Schisandra chinensis* peptidoglycan-assisted transmembrane transport of lignans uniquely altered the pharmacokinetic and pharmacodynamic mechanisms in human HepG2 cell model. *PLoS One* **9**, e85165. https://doi.org/10.1371/journal.pone.0085165 (2014).
98. Olejniczak, A. B. et al. Infrared spectroscopy of nucleoside and DNA-oligonucleotide conjugates labeled with carborane or metallacarborane cage. *Vib. Spectrosc.* **39**, 177–185 (2005).
99. Liao, Y. et al. Study on extraction and antibacterial activity of aucubin from *Eucommia ulmoides* seed-draff waste biomass. *Heliyon* **8**, e10765. https://doi.org/10.1016/j.heliyon.2022.e10765 (2022).
100. Nalbandian, L. et al. Magnetic nanoparticles in medical diagnostic applications: synthesis, characterization and proteins conjugation. *Curr. Nanosci.* **12**, 455–468 (2016).
101. Yew, Y. P. et al. Green synthesis of magnetite (Fe3O4) nanoparticles using seaweed (*Kappaphycus alvarezii*) extract. *Nanoscale Res. Lett.* **11**, 276. https://doi.org/10.1186/s11671-016-1498-2 (2016).
102. Chaki, S. H. et al. Magnetite Fe_3O_4 nanoparticles synthesis by wet chemical reduction and their characterization. *Adv. Nat. Sci. Nanosci. Nanotechnol.* **6**, 035009. https://doi.org/10.1088/2043-6262/6/3/035009 (2015).
103. Segneanu, A. E. et al. *Artemisia annua* growing wild in Romania—A metabolite profile approach to target a drug delivery system based on magnetite nanoparticles. *Plants (Basel)* **10**, 2245. https://doi.org/10.3390/plants10112245 (2021).
104. Sparavigna, A. C. Raman spectroscopy of the iron oxides in the form of minerals, particles and nanoparticles. *ChemRxiv* https://doi.org/10.26434/chemrxiv-2023-22kh4-v2 (2023).
105. Shah, S. T., Yehye, W. A., Chowdhury, Z. Z. & Simarani, K. Magnetically directed antioxidant and antimicrobial agent: synthesis and surface functionalization of magnetite with quercetin. *PeerJ.* **7**, e7651. https://doi.org/10.7717/peerj.7651 (2019).
106. Shah, S. T. et al. Surface functionalization of magnetite nanoparticles with multipotent antioxidant as potential magnetic nanoantioxidants and antimicrobial agents. *Molecules.* **27**, 789. https://doi.org/10.3390/molecules27030789 (2022).
107. Frost, R. L. Raman spectroscopy of natural oxalates. *Anal. Chim. Acta.* **517**, 207–214. https://doi.org/10.1016/j.aca.2004.04.036 (2004).
108. Slavov, L. et al. Raman spectroscopy investigation of magnetite nanoparticles in ferrofluids. *J. Magn. Magn. Mater.* **322**, 1904–1911 (2010).
109. Adar, F. A simple introduction to Raman spectral identification of organic materials. *Spectroscopy* **36**, 8–15 (2021).
110. Karam, J. P., Muscari, C. & Montero-Menei, C. N. Combining adult stem cells and polymeric devices for tissue engineering in infarcted myocardium. *Biomaterials* **33**, 5683–5695. https://doi.org/10.1016/j.biomaterials.2012.04.028 (2012).
111. Ding, S. L. et al. Microcarriers in application for cartilage tissue engineering: Recent progress and challenges. *Bioactive Mater.* **17**, 81–108. https://doi.org/10.1016/j.bioactmat.2022.01.033 (2022).
112. Handral, H. K., Wyrobnik, T. A. & Lam, A.T.-L. Emerging trends in biodegradable microcarriers for therapeutic applications. *Polymers* **15**, 1487. https://doi.org/10.3390/polym15061487 (2023).
113. Ma, M. et al. Magnetic microcarriers with accurate localization and proliferation of mesenchymal stem cell for cartilage defects repairing. *ACS Nano* **17**, 6373–6386. https://doi.org/10.1021/acsnano.2c10995 (2023).
114. Poinern, G. E. J., Halim, A. F. F., Fawcett, D., Chapman, P. & Sharma, R. *Banksia Ashbyi*-engineered facile green synthesis of magnetite nanoparticles: characterization, and determination of micro-strain, stress, and physical parameters by X-ray-based Williamson-Hall analysis. *AIMS Mater. Sci.* **11**, 1096–1124. https://doi.org/10.3934/matersci.2024053 (2024).
115. Souza, T. et al. A comparison of TEM and DLS methods to characterize size distribution of ceramic nanoparticles. *J. Phys. Conf. Ser.* **733**, 012039. https://doi.org/10.1088/1742-6596/733/1/012039 (2016).
116. Narayanaswamy, V. et al. Role of magnetite nanoparticles size and concentration on hyperthermia under various field frequencies and strengths. *Molecules* **26**, 796. https://doi.org/10.3390/molecules26040796 (2021).
117. Li, Q. et al. Correlation between particle size/domain structure and magnetic properties of highly crystalline Fe_3O_4 nanoparticles. *Sci. Rep.* **7**, 9894. https://doi.org/10.1038/s41598-017-09897-5 (2017).
118. Gulcin, İ. Antioxidants and antioxidant methods: an updated overview. *Arch. Toxicol.* **94**, 651–715. https://doi.org/10.1007/s00204-020-02689-3 (2020).
119. Abdullah, J. A. A. et al. Green synthesis of FexOy nanoparticles with potential antioxidant properties. *Nanomaterials (Basel)* **12**, 2449. https://doi.org/10.3390/nano12142449 (2022).
120. Kunjan, F. et al. Evaluation of free radical scavenging and antimicrobial activity of *Coleus amboinicus*-mediated iron oxide nanoparticles. *Cureus* **16**, e55472. https://doi.org/10.7759/cureus.55472 (2024).
121. Jadid, N. et al. Antioxidant activities of different solvent extracts of Piper retrofractum Vahl. using DPPH assay. *AIP Conf. Proc.* **1854**, 020019. https://doi.org/10.1063/1.4985410 (2017).
122. Kamiloglu, S., Sari, G., Ozdal, T. & Capanoglu, E. Guidelines for cell viability assays. *Food Front.* **1**, 332–349. https://doi.org/10.1002/fft2.44 (2020).
123. Gavanji, S., Bakhtari, A., Famurewa, A. C. & Othman, E. M. Cytotoxic activity of herbal medicines as assessed in vitro: A review. *Chem. Biodivers.* **20**, e202201098. https://doi.org/10.1002/cbdv.202201098 (2023).
124. Aslantürk, Ö. S. *In vitro* cytotoxicity and cell viability assays: principles, advantages, and disadvantages. In *Genotoxicity* (ed. Larramendy, M. L.) (InTech, 2018).

125. Mikaeili Ghezeljeh, S. et al. Iron oxide nanoparticles coated with glucose and conjugated with safranal (Fe_3O_4@Glu-Safranal NPs) inducing apoptosis in liver cancer cell line (HepG2). *BMC Chem.* **18**, 33. https://doi.org/10.1186/s13065-024-01142-1 (2024).
126. Roemhild, K. et al. Iron metabolism: pathophysiology and pharmacology. *Trends Pharmacol. Sci.* **42**, 640–656. https://doi.org/10.1016/j.tips.2021.05.001 (2021).
127. Segneanu, A. E. et al. Highly efficient engineered waste eggshell-fly ash for cadmium removal from aqueous solution. *Sci. Rep.* **12**, 9676. https://doi.org/10.1038/s41598-022-13664-6 (2022).
128. Somaida, A. et al. Potent cytotoxicity of four cameroonian plant extracts on different cancer cell lines. *Pharmaceuticals* **13**, 357. https://doi.org/10.3390/ph13110357 (2020).
129. Segneanu, A. E. et al. Wild-grown Romanian *Helleborus purpurascens* approach to novel chitosan phyto-nanocarriers—Metabolite profile and antioxidant properties. *Plants* **12**, 3479. https://doi.org/10.3390/plants12193479 (2023).
130. Kar, S. et al. Expression profiling of DNA methylation-mediated epigenetic gene-silencing factors in breast cancer. *Clin. Epigenet.* **6**, 20. https://doi.org/10.1186/1868-7083-6-20 (2014).

Acknowledgements

This work was supported by a grant from the European Research Executive Agency, Topic: HORIZON-MSCA-2022-SE-01-01, Type of action: HORIZON TMA MSCA Staff Exchanges, Project: 101131420 Exploiting the multifunctional properties of polyphenols: from wastes to high value products, Acronym: PHENOCYCLES.

Author contributions

Conceptualization: A.-E.S., C.S., L.-E.B., and C.B.; methodology: A.-E.S., G.V., C.N.M., T.V., D.D.H., M.V.C., A.E.M., C.M.Z., V.S., and C.S.; writing—original draft preparation: A.-E.S., C.S., and L-.E.B.; writing—review and editing: A.-E.S., D.D.H., L.-E.B., and C.B.; supervision, A.-E.S., L.-E.B., and C.B.; All authors have read and agreed to the published version of the manuscript.

Declarations

Competing interests

The authors declare no competing interests.

Additional information

Supplementary Information The online version contains supplementary material available at https://doi.org/10.1038/s41598-025-92495-7.

Correspondence and requests for materials should be addressed to L.-E.B.